Master's Thesis

Study of Controlling Secondary Building Units of Metal-organic Frameworks

Jaehui Kim

Department of Chemistry

Ulsan National Institute of Science and Technology

2021

Study of Controlling Secondary Building Units of Metal-organic Frameworks

Jaehui Kim

Department of Chemistry

Ulsan National Institute of Science and Technology

2021

Study of Controlling Secondary Building Units of Metal-organic Frameworks

A thesis/dissertation submitted to
Ulsan National Institute of Science and Technology
in partial fulfillment of the
requirements for the degree of
Master of Science

Jaehui Kim

01/13/2021

Approved by

Advisor
Hoi Ri Moon

Study of Controlling Secondary Building Units of Metal-organic Frameworks

Jaehui Kim

This certifies that the thesis/dissertation of Jaehui Kim is approved.

01/13/2021

Advisor: Hoi Ri Moon

Myoung Soo Lah

Wonyoung Choe

Abstract

A class of metal-organic frameworks (MOFs) were constructed by polynuclear metal clusters (secondary building units; hereinafter, SBUs) and their coordination with organic linkers (i.e., ligands). Such MOFs have been widely used in the various applications fields such as gas storage and separation, chemical sensing, and catalysis due to their stable structures and possibility of having a diverse set of functions. To make such MOFs have specific functions applicable to the application fields, we need to synthesize MOFs with specific crystal structures by controlling the two determinants of the crystal structures – the SBUs *per se* and/or their coordination with ligands. In this thesis, we reported the two research on controlling SBUs of MOFs. One research deals with the transformation of SBUs in synthesizing a rarely reported ndc-based Zn MOF. The other research deals with the formation of SBUs in synthesizing bdc-based Zn MOFs. For each research, we identified the set of parameters that facilitate the synthesis of MOFs with specific SBUs.

First, we conducted the transformation of SBUs in synthesizing a rarely reported ndc-based Zn MOF. We transformed specific MOFs –Zn MOFs having four handed paddlewheel SBUs linked by N-donor pillars – into another MOF – MOF having 7-coordinated $Zn_4O(COO)_7$ SBUs. We found that the two parameters – the presence of Zn^+-O^- in solution and the basicity of ligands – affect the transformation of SBUs. First, the presence of Zn^+-O^- in solution facilitates the transformation of SBUs. We conducted the transformation of the two same Zn-MOFs in two different solutions – one solution contains Zn^+-O^- in solution and the other solution does not contain Zn^+-O^- in solution. We found that the Zn-MOF in a solution containing Zn^+-O^- were transformed into the MOF that we want to obtain (i.e., MOF having 7-coordinated $Zn_4O(COO)_7$ SBUs) but the Zn-MOF in the other solution did not. Second, low basicity of ligands facilitates the solid-state transformation. We synthesized three Zn-MOFs by making each of them have different basicity of ligands and found that a Zn-MOF with a low level of basicity of ligands was successfully transformed into the other MOF that we want to obtain (i.e., a MOF having 7-coordinated $Zn_4O(COO)_7$ SBUs).

We also conducted the formation of diverse SBUs in synthesizing bdc-based Zn MOFs (bdc = benzene-1,4-dicarboxylate). We found that the two parameters – the reaction temperature and the molar ratio of precursors (i.e., metal precursors and ligand precursors)– influence the determination of the SBUs of the bdc-based Zn-MOFs .We found that at lower temperature, a Zn-MOF having $Zn_3(COO)_6$ SBUs was

successfully formed. Secondly, we found that molar ratio of metal precursors to ligand precursors affects the formation of bdc-based Zn-MOFs. At the molar ratio of $Zn(NO_3)_2 \cdot 6H_2O$: H_2bdc = 1 : 2, a Zn-MOF having $Zn_3(COO)_6$ SBU, to which two terminal DMF solvents are coordinated, was obtained. At the molar ratio of $Zn(NO_3)_2 \cdot 6H_2O$: H_2bdc = 1 : 4, the other Zn-MOF having $Zn_3(COO)_6(COOH)_2$ SBU (Not surely determined), which is linked by bdc pillars, was obtained.

After studying how to synthesize MOFs, we further explored the possibility of using the MOF that is synthesized by the above-mentioned transformation of SBUs (i.e., 7C-MOF) for CO_2 cycloaddition. 7C-MOF has been rarely reported in the academic field, so exploring the characteristics of this MOF that can be applicable into the "real" world may contribute to expanding the usage of 7C-MOF. We analyzed 7C-MOF using CO_2 sorption isotherm and found that 7C-MOF is capable of adsorbing CO_2 molecules. This is because 7C-MOF is an anionic framework and has cation complex $[Zn(DMF)_6]^{2+}$ in its pores. Thus, we expected that 7C-MOF can act as a Lewis catalyst for CO_2 cycloaddition. By analyzing product yields (100[mole of cyclic carbonate] / [mole of cyclic carbonate and epoxide]) using H-nuclear magnetic resonance spectroscopy, we found that 7C-MOF can act as a Lewis acid catalyst which facilitates CO_2 cycloaddition.

Table of Contents

Nomenclatures

MOF	Metal-organic framework
PXRD	Power X-ray diffraction
SCXRD	Single-crystal X-ray diffraction
TGA	Thermogravimetric analysis
EA	Elemental analysis
FT-IR	Fourier Transform Infrared Spectroscopy
BET	Brunauer-Emmett-Teller
^{1}H-NMR	H-nuclear magnetic resonance spectroscopy
DMF	N, N-dimethylformamide
DEF	N, N-diethylformamide
H_2ndc	1,4-naphthalene dicarboxylic acid
H_2bdc	1,4-benzene dicarboxylic acid
dpndi	N, N'- di-4-pyridylnaphthalenetetracarboxydiimide
bpy	4, 4'-bipyridine
dabco	1,4-diazabicycle[2,2,2]octane
CO_2	Carbon dioxide
SBU	Secondary building unit

List of Figures and tables

1 General Introduction

Metal-organic frameworks (MOFs) consist of mononuclear/polynuclear metal clusters and their coordination with organic linkers (Figure 1.1). Compared to MOFs with mononuclear metal clusters, MOFs with polynuclear metal clusters have more robust structures that are less likely to be changed. This is because multiple metal ions are strongly entangled with each other through linking themselves with ligands when forming a MOF, which helps the MOF have SBUs with their fixed coordination geometries.

The polynuclear metal clusters are commonly referred to as secondary building units (hereinafter, SBUs) when those polynuclear metal clusters are linked with each other through ligands to form a MOF. The crystal structures of MOFs with SBUs can be more diversely constructed than others because various components can be used as SBUs and various types of coordination can exist between the SBUs and ligands. Thus, we can design and synthesize a MOF having a function, which is inherent to its specific crystal structure, without limitation on the set of possible functions that we can impose on the MOF. Due to their stable structures and possibility of having a diverse set of functions, such MOFs have been promising materials for applications such as gas storage and separation [1-4], drug delivery [5-6], and catalysis [7-9]. For example, MOFs can have a function of separating propylene, which can be used for making petrochemical products, from propylene/propane mixture [4], carrying drugs and releasing them into a target part of our body [5], or facilitating the conversion of CO_2 into cyclic carbonate which can be electrolyte solvents [9].

To make such MOFs have specific functions applicable to those fields, we need to synthesize a MOF with a specific crystal structure by controlling the two determinants of the crystal structures – the SBUs *per se* and/or their coordination with ligands. In this thesis, we introduced two methods of synthesizing a MOF with a specific structure**. In the section 2**, we introduced the solid-state transformation which transforms a MOF with a specific crystal structure into another MOF with another crystal structure. **In the section 3,** we introduced the topology control of a MOF when synthesizing the MOF with a specific crystal structure at once (i.e., one step). **In the section 4,** we introduced one of the application fields – CO_2 cycloaddition – for which a MOF synthesized by the solid-state transformation can be used.

2 Transformation of SBUs in Synthesizing a ndc-based Zn MOF

2.1 Introduction

Because the application areas of MOFs are becoming wide, designing and synthesizing MOFs with specific functions applicable to those application areas are required. However, the synthesis of MOFs with specific structures are quite difficult. The main issue regarding the synthesis is that the crystal structures of MOFs are often randomly decided when synthesizing MOFs at once. To address this limitation, researchers have transformed a MOF with a specific crystal structure (i.e., *ex-ante* MOF) into another MOF with another specific crystal structure (i.e., *ex-post* MOF) by adjusting parameters that significantly change the crystal structure of the *ex-ante* MOF [10-16]. Thus, to obtain a MOF with a specific function, it is important to identify the parameters and study the ways of adjusting them.

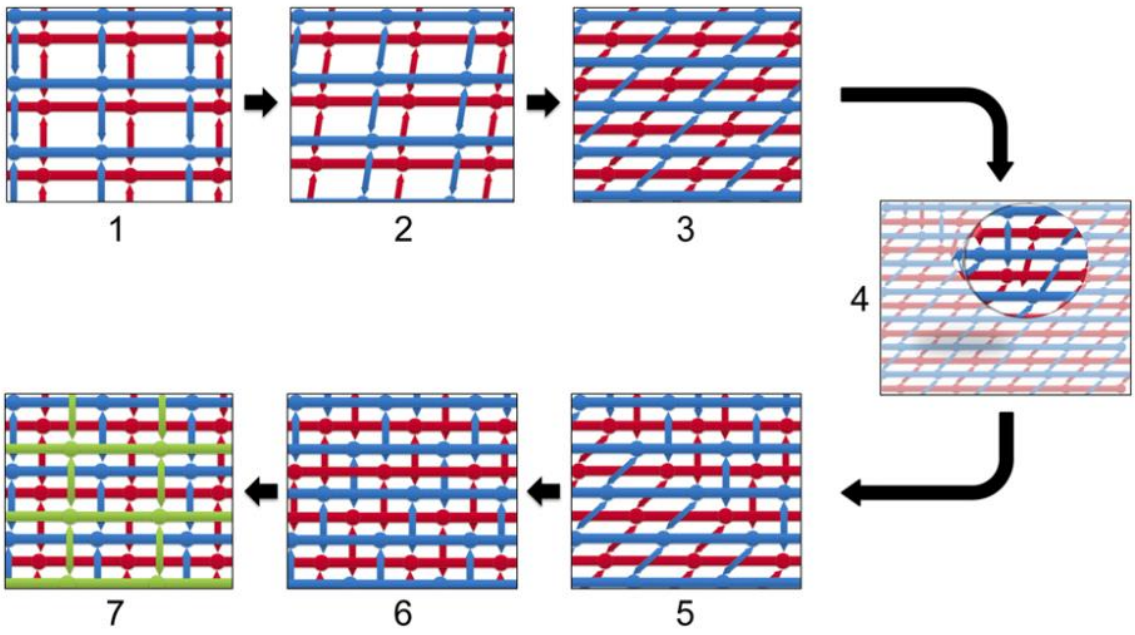

Figure 2.1 Schematic illustration of the solid-state transformation from the doubly interpenetrated $[Zn_2(bdc)_2(bpy)]_n$ to the triply interpenetrated $[Zn_2(bdc)_2(bpy)]_n$ [10].

By Barbour et al., a doubly interpenetrated ndc-based Zn MOF having bipyridine as a pillar was transformed into a triply interpenetrated MOF in the solid state (Figure 2.1) [10]. The solid-state transformation was triggered by desolvation of the doubly interpenetrated $[Zn_2(ndc)_2(bpy)]_n$ MOF at 120 °C. In the progress of the desolvation, two-dimensional layers that were formed by linking SBUs

with ndc ligands can slide while keeping their original connectivity between ndc ligands and SBUs, and the coordination between zinc metal ions and bpy broke down and regenerated.

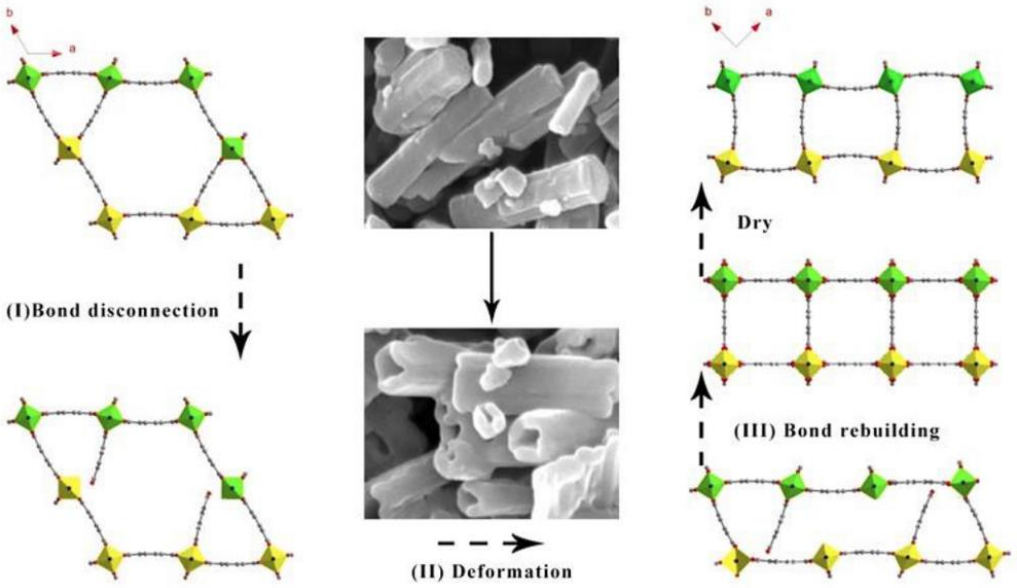

Figure 2.2 Solid-state transformation of the lattice fom from the kagomé to the square. Methanol causes the transformation. [11].

Tao and coworkers transformed the lattice form of Zn MOFs having four handed paddlewheel SBUs, more especially from the kagomé to sqaure shape while keeping their solid state (Figure 2.2) [11]. Added methanol triggers the cleavage and reformation of coordination bonds between the metal nodes and carboxylate groups.

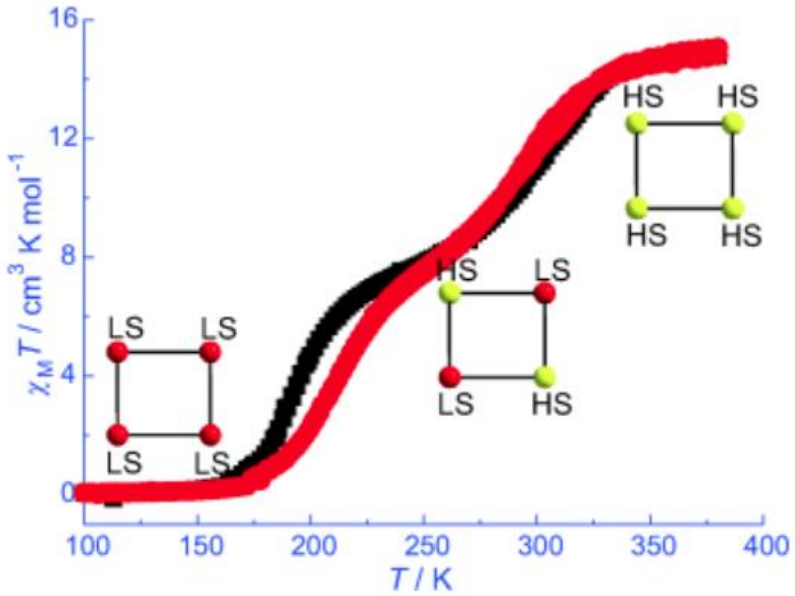

Figure 2.3 Solid-state transformation of Fe^{II}_4 squares having from four low-spin to four high spin centers [12].

Zheng and co-workers conducted research on transforming spin of Fe^{II}_4 squares from having four low-spin to having four high spin centers through the adsorption and desorption process of water molecules (Figure 2.3) [12]. Also, Nakamura's research group conducted a solid-state transformation of MOF-2 ($[Zn(bdc)(H_2O)]_n$) built by 4-coordinated SBUs into MOF-5 ($[Zn_4(\mu_4\text{-}O)(bdc)_3]_n$) built by 6-coordinated SBUs (Figure 2.4) [15, 16]. The research group heats N, N'- dimethyl formamide (DMF) solution containing MOF-2 and zinc ion precursors (i.e., zinc nitrate hexahydrate). Then, the group obtained formate from DMF hydrolysis, which acts as a base. Such increased basicity of the solution produces basic oxide ions (i.e., Zn^+-O^-), resulting in the solid-state transformation.

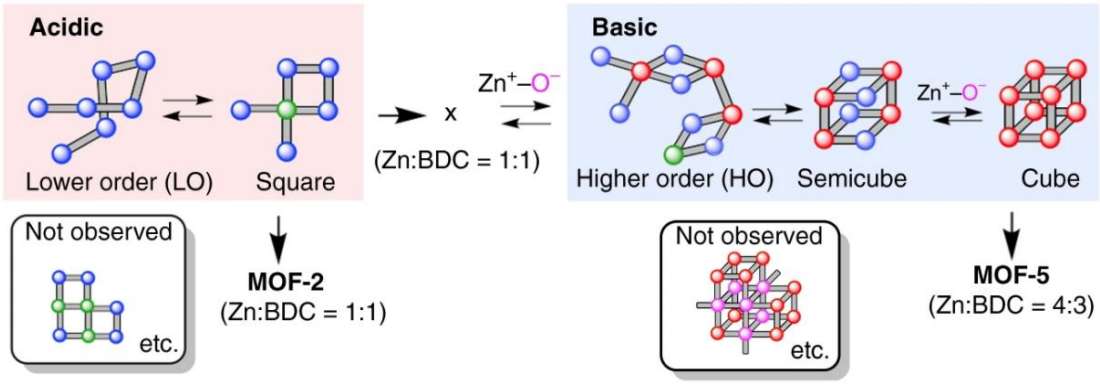

Figure 2.4 Transformation of MOF-2 into MOF-5 [15, 16].

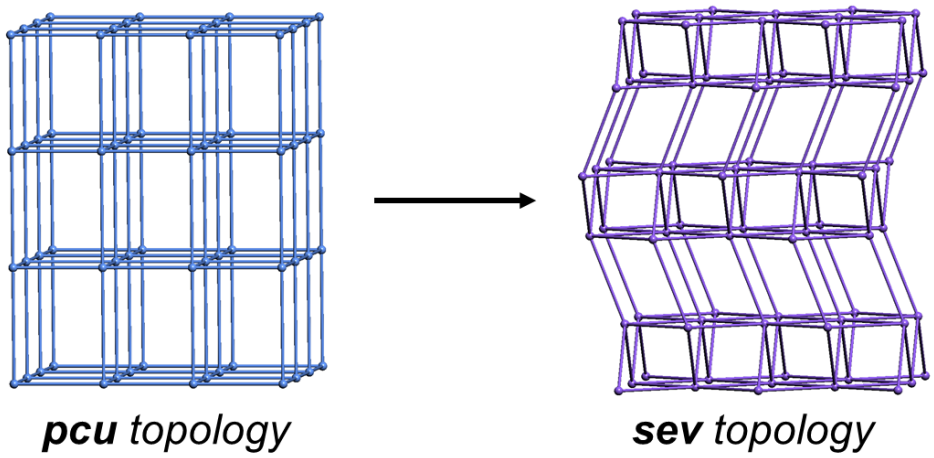

Figure 2.5 Transformation of **pcu** into **sev** topology

Inspired from the experiment of the research group, we expected that the two parameters–basicity of ligands and basic oxide ions in solution–influence cleavages and reformations of coordination between SBUs and ligands, resulting in the solid-state transformations of MOFs. Specifically, we hypothesized that low basicity of ligands makes the transformation more easily happen, and having basic oxide ions in solution facilitates the transformation. To verify my hypothesis, I conducted the solid-state transformations from Zn-MOFs built by 6-coordinated pillared paddlewheel SBUs with **pcu** topology to another Zn-MOF built by 7-coordinated $Zn_4O(COO)_7$ SBUs with **sev** topology (Figure 2.5).

Firstly, to verify that low basicity of ligands facilitates solid-state transformations, we used the following three Zn-MOFs with **pcu** topology which have different basicity of ligands as *ex-ante* MOFs: (1) a MOF of Zn-MOFs with **pcu** topology is $[Zn_2(ndc)_2(dpndi)]_n$ (ndc = 1,4-naphthalene dicarboxylate; dpndi = N,N'- di-4-pyridylnaphthalenetetracarboxydiimide) (i.e., a MOF which has low basicity – pK_a = 3.92 – of ligands), (2) a MOF of Zn-MOFs with **pcu** topology is $[Zn_2(ndc)_2(bpy)]_n$ (i.e., a MOF which has moderate basicity – pK_a = 5.25 – of ligands), (3) a MOF of Zn-MOFs with **pcu** topology is $[Zn_2(ndc)_2(dabco)]_n$ (dabco = 1,4 = diazabicycle[2,2,2]octane) (i.e., a MOF which has high basicity – pK_a = 9.76 – of ligands). Through the transformation of each Zn-MOFs with **pcu** topology, I could successfully obtain a Zn-MOF with **sev** topology from $[Zn_2(ndc)_2(dpndi)]_n$ and $[Zn_2(ndc)_2(bpy)]_n$ (i.e., a MOF with low or moderate basicity) but not from $[Zn_2(ndc)_2(dabco)]_n$ (i.e., a MOF with high basicity).

Secondly, to verify basic oxide ions in a solution facilitate solid-state transformations, we used the $[Zn_2(ndc)_2(bpy)]_n$ MOF and conducted solid-state transformations of the MOF either (1) in DMF containing zinc nitrate hexahydrate (i.e., the presence of basic oxide ions in the solution) or (2) in DMF containing no zinc nitrate hexahydrate (i.e., the absence of basic oxide ions in the solution). Trough the solid-state transformations of $[Zn_2(ndc)_2(bpy)]_n$ MOF with **pcu** topology, we could successfully obtain a Zn-MOF with **sev** topology built by 7-coordinated $Zn_4O(COO)_7$ SBUs from $[Zn_2(ndc)_2(bpy)]_n$ MOF in DMF containing zinc nitrate hexahydrate (i.e., the presence of basic oxide ions in the solution) but not from the same MOF in DMF containing no zinc nitrate hexahydrate (i.e., the absence of basic oxide ions in the solution).

For each transformation described above, we checked whether a Zn-MOF with **sev** topology built by 7-coordinated $Zn_4O(COO)_7$ SBUs is successfully made using powder and single-crystal X-ray diffraction.

2.2 Experimentation

2.2.1 Materials and instruments

UNIST Central Research Facilities center in Ulsan National Institute of Science and Technology helps us to conduct elemental analyses. The single crystal was coated with Parabar 10312 (Hampton Research Inc.) to mount micro-loop. We used synchrotron employing a PLSII-2D SMC an Rayonix MX225HS detector with a silicon (111) double crystal monochromator (DCM) at Pohang Accelerator Laboratory, Korea to collect SCXRD data measured using. The 8 PAL BL2D-SMDC program [18] was used for both data collection, and HKL3000sm (Ver. 730r) [19] was used for cell refinement, reduction and absorption correction. The crystal structures were solved by the intrinsic phasing method with SHELX-XT (Ver. 2018/2) [20], and refined by full-matrix least-squares calculation with SHELX-XL (Ver. 2018/3) [21]. All non-hydrogen atoms in whole structures were refined anisotropically. Although some structure solvents were observed by Fourier Mapsin the X-ray diffraction, the exact position of these solvent molecules could not be well defined due to disordered solvent of diffused electron densities. We used the SQUEEZE routine in the software of PLATON [22] and performed the final structure refinements. The additional crystallographic data are summarized in Table 2.1, and CCDC 1986596 also contain the supplementary crystallographic data for this paper. The data can be obtained free of charge at www.ccdc.cam.ac.uk/conts/retrieving.html or from the Cambridge Crystallographic Data Centre, 12, Union Road, Cambridge CB2 EX, UK.

2.2.2 Synthesis of $6C_{bpy}$-MOF

Zinc nitrate hexahydrate (0.074 g, 0.00025 mol), 1,4-naphthalene dicarboxylic acid (0.054 g, 0.00025 mol) and 4, 4’ - bipyridine (0.019 g, 0.000125 mol) were dissolved in DMF solution (5 mL). The solution was heated for two days (80 °C).

2.2.3 Thermal treatment of $6C_{bpy}$-MOF to 7C-MOF

$6C_{bpy}$-MOF (0.030 g, 0.000042 mol) was added into DMF solution (0.005 L) containing zinc nitrate hexahydrate (0.062 g, 0.00021 mol). The mixture was heated for 1.5 days (70 °C). Yield: 20 mg (35%). Calculated by elemental analysis for $Zn_{4.5}C_{61.5}H_{70.5}N_{6.5}O_{23.5}$: C, 47.01; H, 4.52; N, 5.80.; found: C, 46.74; H, 4.27; N, 5.85.

2.2.4 Synthesis of $6C_{dabco}$-MOF

Zinc nitrate hexahydrate (0.476 g, 0.0016 mol), 1,4-naphthalene dicarboxylic acid (0.346 g, 0.0016 mol) were dissolved in DMF solution (0.020 L). dabco (0.09 g, 0.0008 mol) was added to the DMF solution. Using centrifuge, supernatant solution was prepared. The solution was heated for a day (100 °C).

2.2.5 Thermal treatment of $6C_{dabco}$-MOF

$6C_{dabco}$-MOF (0.03 g, 0.000045 mol) was added into DMF solution (0.005 L) containing zinc nitrate hexahydrate (0.268 g, 0.0009 mol). The mixture was heated for 1.5 day (70 °C).

2.2.6 Synthesis of $6C_{dpndi}$-MOF

We modified the procedure conducted by another group [25], zinc nitrate hexahydrate (0.012 g, 0.00004 mol), 1,4-naphthalene dicarboxylic acid (0.009 g, 0.00004 mol), and dpndi (0.017 g, 0.00004 mol) were dissolved in N,N'-diethylformamide (DEF) (0.005 L). The solution was heated for 48 h (70 °C).

2.2.7 Thermal treatment of $6C_{dpndi}$-MOF into 7C-MOF

$6C_{dpndi}$-MOF (0.03 g, 0.000031 mol) was added into DMF solution (0.005 L) containing zinc nitrate hexahydrate (0.045 g, 0.00015 mol). The mixture was heated for 1.5 day (70 °C). Yield: 0.0015 g (5 %)

2.2.8 Synthesis of IRMOF-7

We modified the procedure conducted by another group [26]. Zinc nitrate hexahydrate (0.119 g, 0.00040 mol), 1,4-naphthalenedicarboxylic acid (0.087 g, 0.00040 mol) were dissolved in DEF solution (0.005 L). The solution was heated for a day (100 °C). ‘

2.2.9 Thermal treatment of IRMOF-7 into 7C-MOF

IRMOF-7 (0.046 g, 0.000028 mol) was added to DMF solution (0.005 L) containing 1,4-naphthalene dicarboxylic acid (0.011 g, 0.00005 mol). The solution was heated for a day (100 °C). Yield: 0.037 g (84%).

2.2.10 Synthesis of $[Zn_2(bdc)_2(bpy)]_n$

We modified the procedure conducted by another group [27]. Zinc nitrate hexahydrate (0.088 g, 0.0003 mol), terephthalic acid (0.050 g, 0.00030 mol) and 4,4'-bipyridine (0.023 g, 0.00015 mol) were suspended in DMF and ethanol (1:1 (v/v), 0.025 L), and the mixture was heated for one day (90 °C).

2.2.11 Synthesis of $[Zn_2(2,6\text{-ndc})_2(bpy)]_n$

Considering one synthesis conducted by other group [28], zinc nitrate hexahydrate (0.089 g, 0.0003 mol) and 2,6-naphthalene dicarboxylic acid (0.065 g, 0.00030 mol) were dissolved in DMF/MeOH solution (1:1 (v/v), 0.006 L). 4,4'-bipyridine (0.023 g, 0.00015 mol) was added the solution. We stirred the mixture at R.T. for one day and put for two days (120 °C).

2.3 Results and Discussion

2.3.1 The presence of Zn^{+}-O^{-} in solution

In order to verify our postulation that whether basic oxide ions exist in solution or not affects the solid-state transformation. We firstly prepared $6C_{bpy}$-MOF through the reaction of zinc nitrate hexahydrate (i.e., $Zn(NO_3)_2{\cdot}6H_2O$), ndc, and bpy in the DMF solution, as it is described in one previously reported procedure [23]. After the solvothermal reaction, we obtained colorless large cuboid crystals (Figure 2.6(a)). The MOF we synthesized have octahedrally 6-coordinated Zn-based SBUs and have **pcu** topology. Each square window that is formed by the coordination between the zinc metal and ndc ligands was linked by bpy pillar ligand in a square-pyramidal fashion, resulting in three-dimensional structures (Figures 2.6(a) and Figure 2.7). Furthermore, the MOF has non-interpenetrated crystal structure due to the bulkiness of the ndc ligand. The non-interpenetrated structures provide the possibility of making other solvents or reactants accessible to the SBUs. So, we expected that relatively weak coordination bond of the metal-N-donor can be deformed by the solid-state transformation. [29-33].

To verify the presence of the basic oxide ions affects the topology conversion of the $6C_{bpy}$-MOF, the $6C_{bpy}$-MOF crystals (0.030 g) underwent a solvothermal reaction in placed a DMF solution (5 mL) containing zinc nitrate hexahydrate (~ 5 equivalent per each paddle-wheel SBU) for 1.5 days (70 °C). We added the zinc nitrate hexahydrate in the reaction to derive the generation of the basic oxide ions during the reaction [16, 34]. Through the solid-state transformation, we obtained polycrystalline cuboid crystals (Figure 2.6(b)). We confirmed that the MOF we obtained through the solid-state transformation is the 7C-MOF by comparing the PXRD patterns of $6C_{bpy}$-MOF and the transformed solid (Figure 2.6(d)). Using single-crystal X-ray diffraction (SCXRD) data. We confirmed the exact structure of 7CMOF using single-crystal X-ray diffraction (SCXRD) data. The 7C-MOF confirmed by SCXRD has $Zn_4O(COO)_7$ SBU, and each SBU is coordinated by seven carboxylates and one terminal DMF molecules (Figure 2.6(b) and Figure 2.7(b)). We found the formula by using TGA and EA: $\{[Zn_4(\mu4\text{-}O)(ndc)_{3.5}(DMF)]\cdot[Zn_{0.5}(DMF)_3]\cdot\ 2.5DMF\cdot2H_2O\}n$ and the orthogonal Cmca space group and has a **sev** net topology. As a side note, the 7C-MOF having 7-coordinated SBUs is rarely reported in MOF chemistry [25–29]. We described more details for the crystallographic information of 7C-MOF **in section 2.3.3**

Compared to the previous transformation that was triggered by ~ 5 equivalent $Zn(NO_3)_2{\cdot}6H_2O$, the heat treatment of $6C_{bpy}$-MOF without zinc precursors or smaller amounts of zinc nitrate hexahydrate (~ 0.5 equivalents to each SBU) did not trigger the solid-state transformation and the $6C_{bpy}$-MOF crystals was remaining almost, as revealed by OM and PXRD patterns (Figures 2.8 and 2.9). Based on the results, we concluded that sufficient amount of basic oxide ions are needed to trigger the transformation from **pcu**

topology of $6C_{bpy}$-MOF to **sev** topology of 7C-MOF.

Inspired by the role of basic oxide ions to trigger the solid-state transformation, we also considered the role of acidic molecules (i.e.,the addition of H_2ndc ligands) instead Zn^{2+}precursors. We conducted the transformation of $6C_{bpy}$-MOF in DMF solution containing was conducted with 1,4-naphthalene dicarboxylic acid instead of zinc precursors. There was no transformation in this case. the original crystal structure of $6C_{bpy}$-MOF was remained, despite of the previous research that demonstrates ligand addition into the SBUs and transformation of the MOFs could be expected [30]. Based on our knowledge, cleavage of coordination bonds are entropically favored when the MOFs are exposed to acidic environment. However, in our $6C_{bpy}$-MOF system, $6C_{bpy}$-MOF might keep its original structure because the MOF is thermodynamically stable eenough to obtain stability from the acidity of the H_2ndc ligands (Figure 2.9).

To expand our knowledge for the role of synthetic precursors (i.e., zin and H_2ndc) to transform in the solid-stat, we conducted the solid-state transformation of IRMOF-7 having **pcu** topology into 7C-MOF under the existence of $Zn(NO_3)_2{\cdot}6H_2O$ or H_2ndc was conducted. IRMOF-7 is built by octahedrally 6-coordinated $Zn_4O(COO)_6$ secondary building units coordinated by six ndc ligands and has the same Zn_4O based secondary building units with 7C-MOF. The only difference between IRMOF-7 and 7C-MOF is the 7C-MOF has one additional carboxylate coordinated to each Zn_4O SBU, resulting in a $Zn_4O(COO)_7$ SBU. The IRMOF-7 has Zn_4O SBIs and each SBU is coordinated by six terephthalic acids, making cubic **pcu** topology. IRMOF-7 crystals (46 mg) was added into a DMF solution (5 mL) containing 1,4-naphthalene dicarboxylic acid (~ 2 equivalent to each secondary building units) and make thermal treatment the prepared solution at 100 °C for 24 h. New opaque crystal was obtained as we described in Figure 2.6(b). The crystal structure of the resulting crystal was the same with that of 7C-MOF based on the PXRD patterns (Figure 2.6(e)). While $6C_{bpy}$-MOF has the octahedrally 6-coordinated pillared-paddlewheel SBUs of, IRMOF-7 has the same Zn_4O SBUs of with the 7C-MOF; therefore, the addition of a basic species was not an influential parameters to trigger the solid-state transformation from IRMOF-7 having $Zn_4O(COO)_6$ SBU to 7C-MOF having $Zn_4O(COO)_7$ SBU. Based on our reasoning, added ndc ligands instead of zinc precursors compensate the scare amount of Zn to carboxylate connectivity and generates the 7C-MOF through the transformation of IRMOF-7.

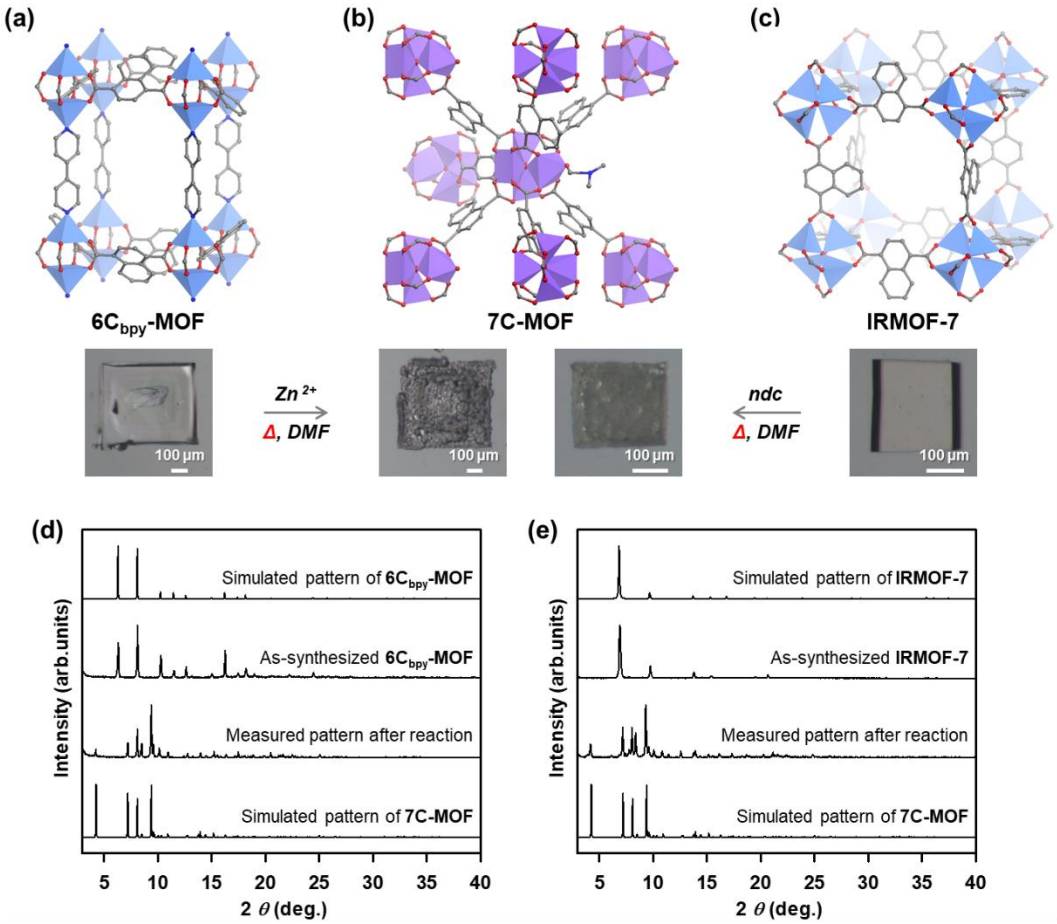

Figure 2.6 Crystal structures and optical microscopic images of (a) $6C_{bpy}$-MOF, (b) 7C-MOF, and (c) IRMOF-7. PXRD patterns describing the transformations from (d) $6C_{bpy}$-MOF to 7C-MOF and IRMOF-7 to 7C-MOF. Color scheme: C, grey; O, red; N, blue; Zn, purple for 7C-MOF and sky blue for other compounds.

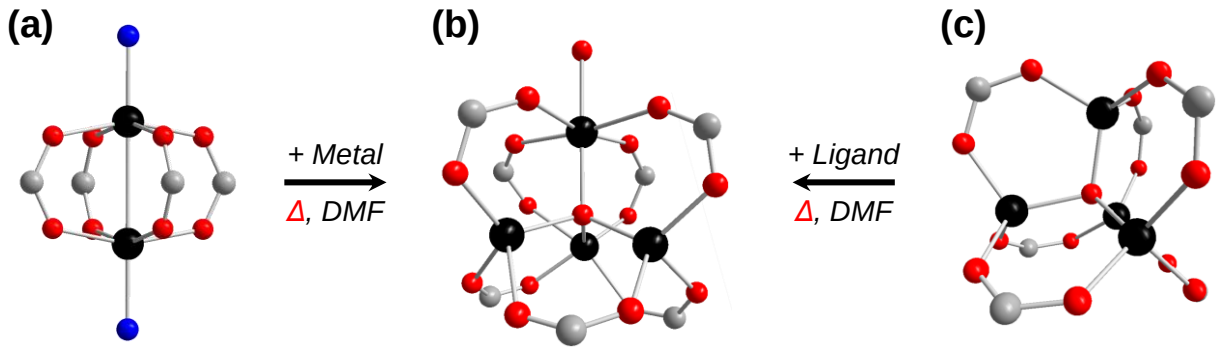

Figure 2.7 Schematic illustrations of SBU geometries of (a) $6C_{bpy}$-MOF, (b) 7C-MOF, and (c) IRMOF-7.

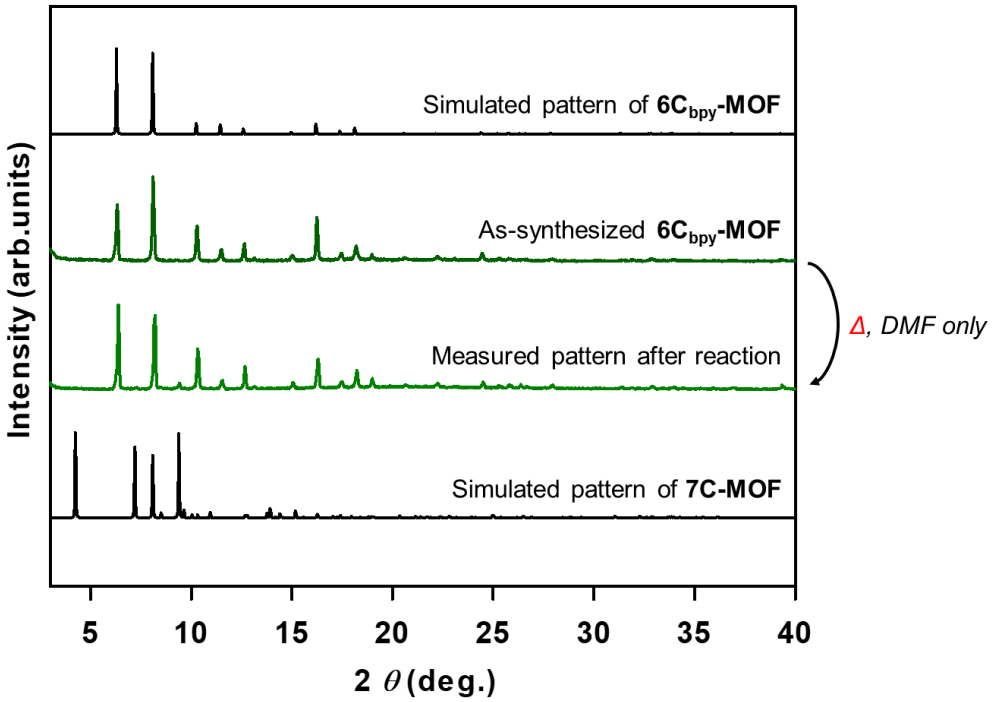

Figure 2.8 PXRD patterns of $6C_{bpy}$-MOF before and after heating in DMF at 70 °C for 36 h. During the transformation reaction, the original phase is well maintained and the peaks corresponding to 7C-MOF do not appear.

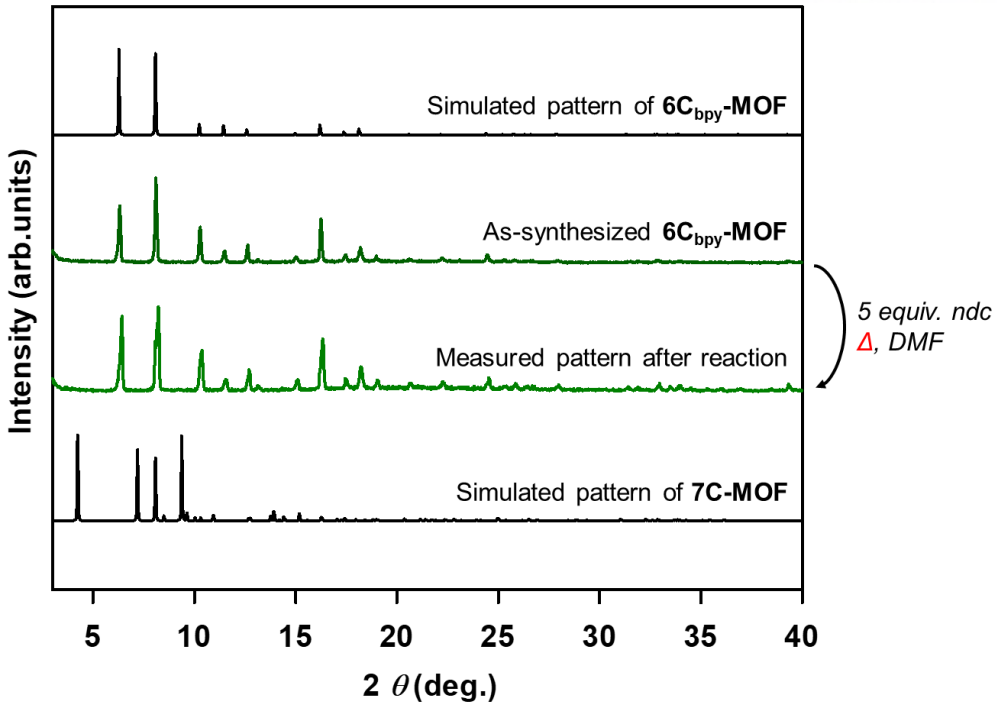

Figure 2.9 PXRD patterns of $6C_{bpy}$-MOF before and after heating in DMF with added ndc (~5 equivalents to each cluster) for 1.5 days (70 °C). During the transformation, the original phase is well maintained and the peaks corresponding to 7C-MOF do not appear.

2.3.2 Basicity of ligands

We also conducted the solid-state transformation of three different types of $6C_L$-MOF (L = pillar molecules to figure out that low basicity of ligands facilitates the solid-state transformations. This is because basicity of ligands decide the relative strength between metal and ligand [32]. To verify our postulation, we used the following three Zn-MOFs with **pcu** topology which have different basicity of ligands as *ex-ante* MOFs: (1) a MOF of Zn-MOFs with **pcu** topology is $[Zn_2(ndc)_2(dpndi)]_n$ (i.e., a MOF which has low basicity – $pK_a = 3.92$ – of ligands), (2) a MOF of Zn-MOFs with **pcu** topology is $[Zn_2(ndc)_2(bpy)]_n$ (i.e., a MOF which has moderate basicity – $pK_a = 5.25$ – of ligands), (3) a MOF of Zn-MOFs with **pcu** topology is $[Zn_2(ndc)_2(dabco)]_n$ (dabco = 1,4 = diazabicycle[2,2,2]octane) (i.e., a MOF which has high basicity – $pK_a = 9.76$ – of ligands) (Figures 2.10(a) and 2.10(b)) [33]. Through the solid-state transformation of each Zn-MOFs with **pcu** topology, I could successfully obtain a Zn-MOF with **sev** topology from $[Zn_2(ndc)_2(dpndi)]_n$ and $[Zn_2(ndc)_2(bpy)]_n$ (i.e., a MOF with low or moderate basicity) but not from $[Zn_2(ndc)_2(dabco)]_n$ (i.e., a MOF with high basicity).

As compared to the previous transformation, a pillared MOF having dabco as a pillar ($6C_{dabco}$-MOF) in a DMF containing zinc nitrate hexahydrate was not successfully transformed into 7C-MOF, even at harsh conditions (20 equivalent of zinc nitrate hexahydrate or harsher temperature (100 °C)). We verified the innerness of $6C_{dabco}$-MOF using PXRD (Figures 2.10 (c) and 2.10 (e) and Figure 2.11). In the contrary, unliked the other pillared MOF, $6C_{dpndi}$-MOF having dpndi as a pillar has strong basic pillars (15.450, 2.569, and 7.043 Å for dpndi, dabco, and bpy, respectively) and their conjugate acid has the relatively low pKa (i.e., weaker base).

$6C_{dpndi}$-MOF underwent the solid-state transformation into 7C-MOF (Figures 2.10(d) and 2.10(f), and Figure 2.12) even though lower concentration of zinc nitrate hexahydrate (0.5 equivalent) was added for the transformation. We reasoned that the basicity of ligands determines the inertness of secondary building units and become determines of if the initial crystal maintains its original for or is transformed to 7C-MOF.

At the above, we described the basicity of ligands impact on the transformation of topology from a MOF having **pcu** topology to another MOF having **sev** topology. Here, we also investigated the effect of carboxylate ligands on the topology conversion. We synthesized other pillared MOFs, $[Zn_2(bdc)_2(bpy)]_n$ and $[Zn_2(2,6\text{-}ndc)_2(bpy)]_n$ [34, 35], and conducted their solid-state transformation under the same solvothermal condition. Noticeably, they have the **pcu** topology which is the same as one of the $6C_{bpy}$-MOF. However, they are doubly interpenetrated because the terephthalic acid and 2,6-naphthalene dicarboxylic acids ligands are not no sterically bulky [36, 37]. The bdc-based MOF was transformed into MOF-5 having

pcu topology, instead of 7C-MOF having the **sev** topology (Figure 2.13). The different results from the ndc-based MOF is maybe because the different characteristic of bdc and ndc ligands. $[Zn_2(2,6\text{-ndc})_2(bpy)]_n$ maintained its original form without any transformation while heating with DMF (Figure 2.14). We reasoned that such inertness of $[Zn_2(2,6\text{-ndc})_2(bpy)]_n$ results from the higher value of pKa of 2,6-naphthalene dicarboxylic acid ligands and triply interpenetrations of the framework making hard to ligand replacement [38]. From the above results, we concluded that the characteristics of the carboxylate ligand is one of the influential parameters to decide whether the conversion of **pcu** to **sev** topology happens or not.

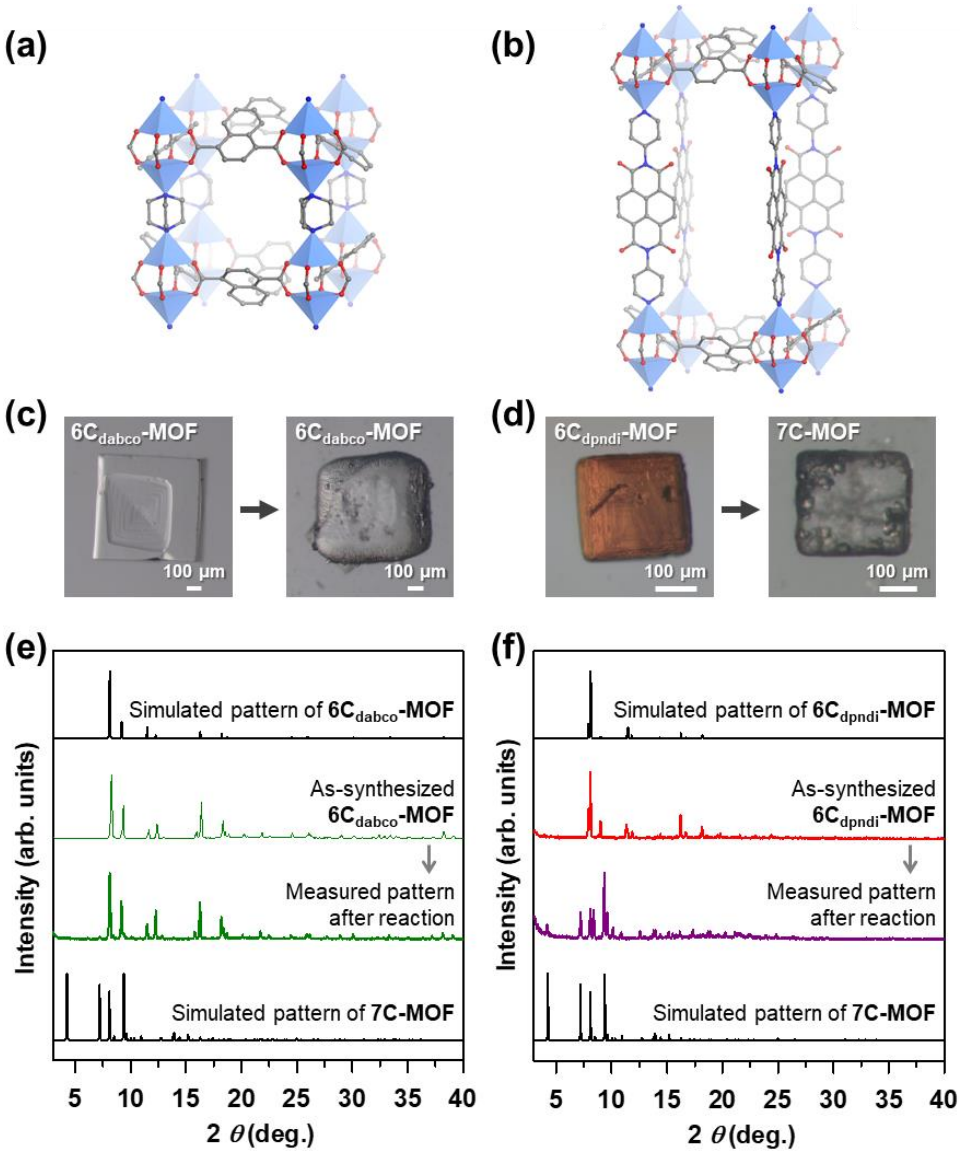

Figure 2.10 Crystal structures and optical microscopic images of (a) 6C$_{dabco}$-MOF and (b) 6C$_{dpndi}$-MOF. PXRD patterns before and after the corresponding transformation reaction for (c and e) 6C$_{dabco}$-MOF and (d and f) 6C$_{dpndi}$-MOF.

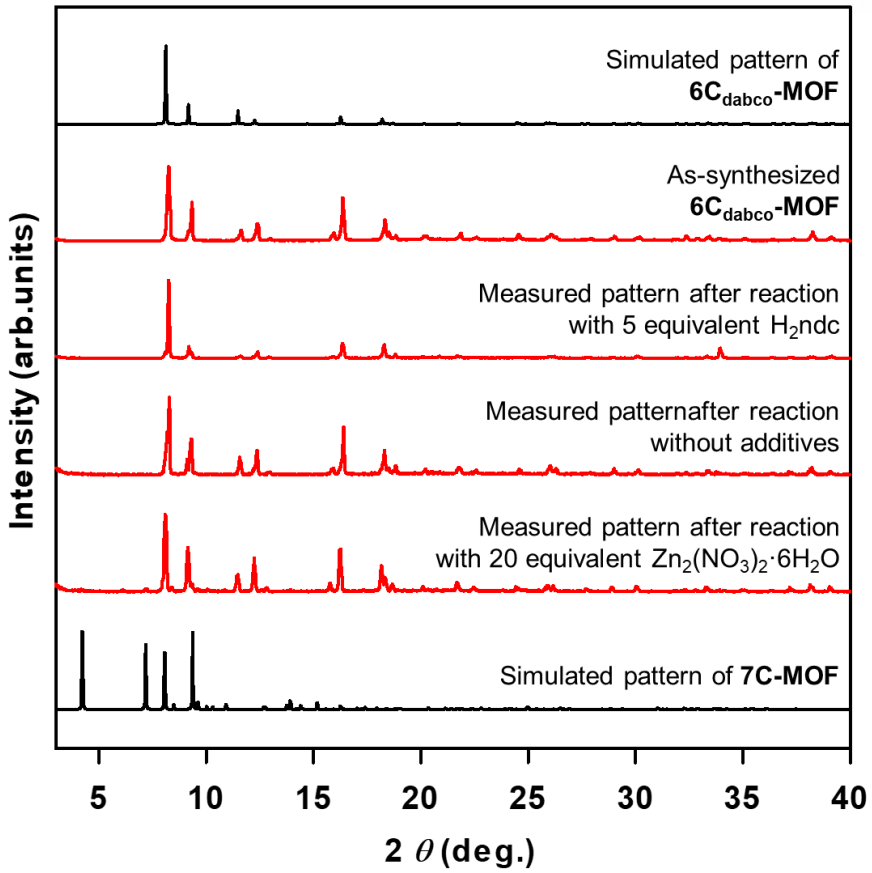

Figure 2.11 PXRD patterns of $6C_{dabco}$-MOF before and after heating in DMF at 70 °C for 36 h with or without corresponding additives. During the transformation reactions, the original phase is well maintained and the peaks corresponding to 7C-MOF do not appear.

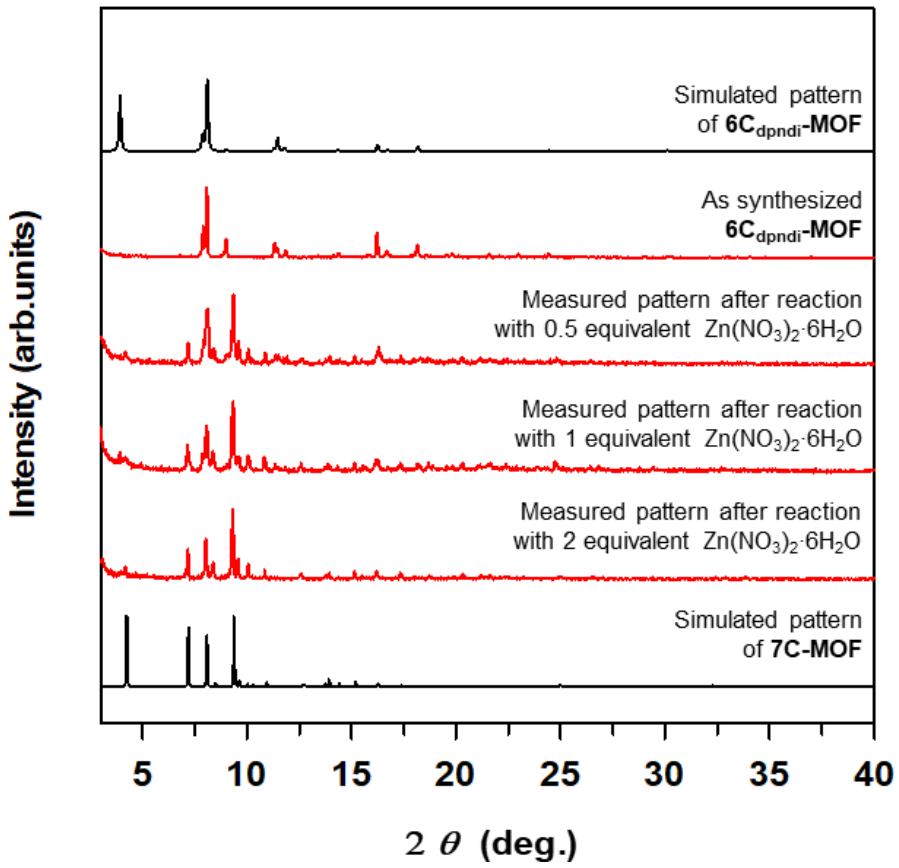

Figure 2.12 PXRD patterns of $6C_{dpndi}$-MOF before and after heating in DMF at 70 °C for 36 h with corresponding amounts of $Zn(NO_3)_2 \cdot 6H_2O$. Upon the solvothermal reactions, the phase transformation to 7C-MOF occurs.

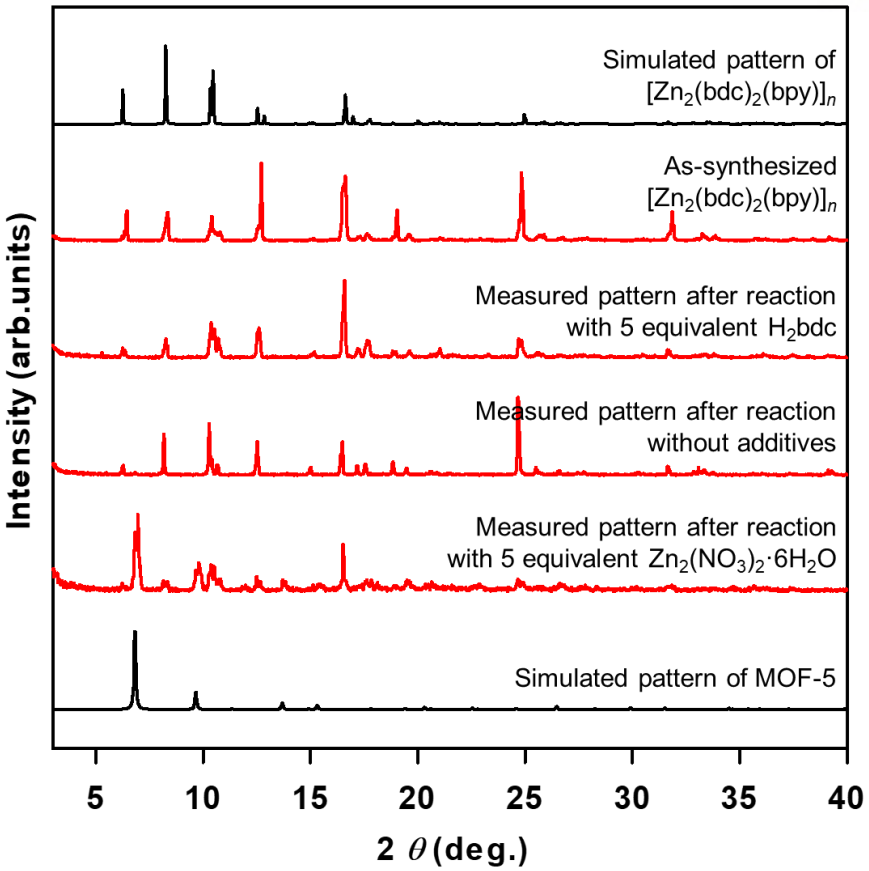

Figure 2.13 PXRD patterns of $[Zn_2(bdc)_2(bpy)]_n$ before and after heating in DMF at 70 °C for 36 h with or without corresponding additives. Upon the solvothermal reaction with ~5 equivalent zinc nitrate hexahydrate, the conversion to MOF-5 occurs.

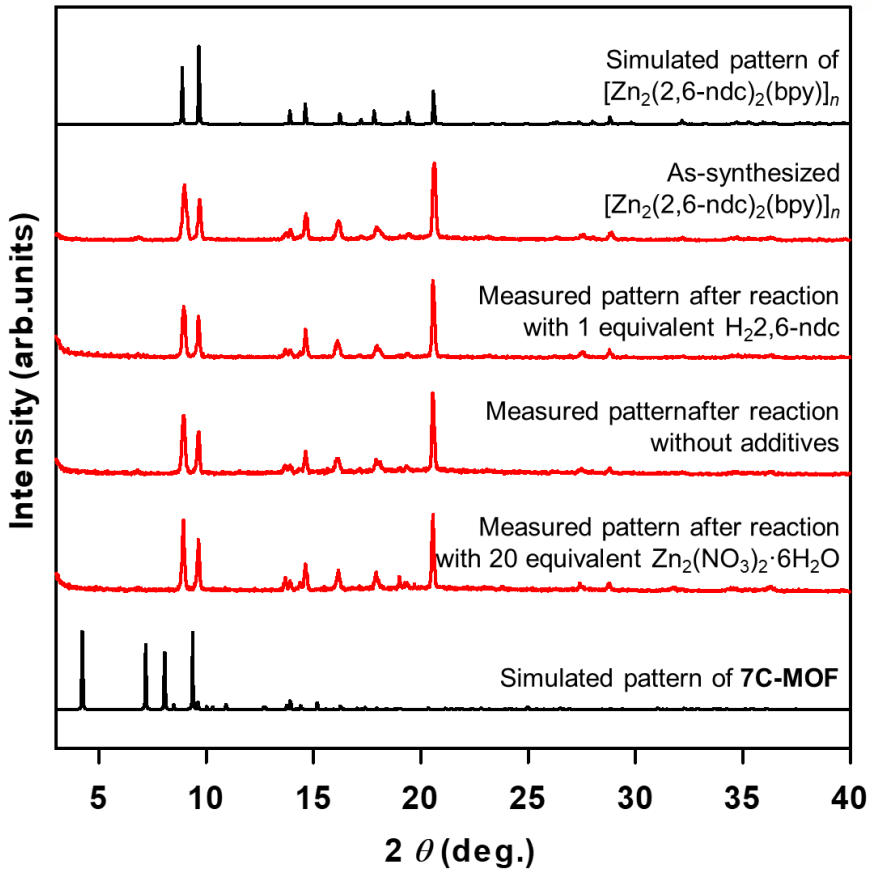

Figure 2.14 PXRD patterns of $[Zn_2(2,6\text{-ndc})_2(bpy)]_n$ before and after heating in DMF at 70 °C for 36 h with or without corresponding additives (2,6-ndc = 2,6-naphthalene dicarboxylate). During the transformation reaction, the original phase is well maintained and the peaks corresponding to 7C-MOF do not appear.

2.3.3 Crystallographic information of 7C-MOF

Through solid-state transformation of pillared MOFs, our group obtained 7C-MOF having $Zn_4O(COO)_7$ SBUs. There are only few MOFs having 7-coordinated SBUs synthesized [39-43]. Liu group and co-workers. reported the **sev** topology which is the same one of the 7C-MOF we synthesized [39], in which Zn^{2+} based SBUs are coordinated with seven ndc^{2-} ligands but the bridging oxygen existing in the secondary building units was different from the reported one because the other group assigned not μ4-O but μ4-OH. In the 7C-MOF, zinc based secondary building units are coordinated by 7 ndc organic linkers and 1 terminal DMF molecule (Figure 2.15 and Figure 2.16). In each SBU, two Zn nodes have four-connected tetragonal geometries and the other Zn nodes have a five-connected square pyramidal geometry and a six-connected tilted octahedral geometry due to the DMF molecule which is coordinated. The charge imbalance issue of 7C-MOF was compensated by the cation complex $[Zn(DMF)_6]^{2+}$ in the pores of the anionic framework (Figure 2.6(b)). The characteristic was verified by the EA (Table 2.2), and SCXRD (Table 2.1).

We used thermogravimetric analysis (TGA) to verify that the coordinated DMF molecules with the guest solvents are removed after heating 7C-MOF. We verified that the weight loss of the 7C-MOF while heating from room temperature to ~270 °C has good agreement with the calculated results (32.5%), which implies that 6.5 DMF molecules and two H_2O molecules per formula unit were lost (Figure 2.17). As a side note, irreversible structural deformation was happened when the sample was heated at 270 °C (Figure 2.18), for activation of the 7C-MOF make the removal of non-coordinating solvent molecules. The activation condition is under vacuum at R.T. The fact is verified by ^{1}H-NMR (Figure 2.19).

Table 2.1 X-ray crystallographic data of **7C-MOF**.

Compound	**7C-MOF**
formula	$C_{108}H_{98}N_8O_{38}Zn_9$
crystal system	*Orthorhombic*
space group	*Pmca*
Formula weight	2704.27
a, Å	17.443(4)
b, Å	18.819(4)
c, Å	40.617(8)
α, deg	90
V, Å^3	13333(5)
Z	4
ρ_{calcd}, g cm^{-3}	1.347
temp , K	173(2)
λ, Å	0.70000
μ, mm^{-1}	1.595
goodness-of-fit (F^2)	1.110
F(000)	5504
reflections collected	77394
independent reflections	11931 [*R*(int) = 0.1432]
completeness to θ_{max}, %	100.0%
data/restraints/parameters	11931 / 157 / 574
θ range for data collection, deg	1.644 to 33.687
Diffraction limits (*h*, *k*, *l*)	$-24 \le h \le 24$, $-28 \le k \le 28$, $-61 \le l \le 61$
refinement method	Full-matrix least-squares on F^2
R_1, wR_2 [$I>2\sigma(I)$]	R_1 = 0.1186[a], wR_2 = 0.3453[b]
R_1, wR_2 (all data)	R_1 = 0.1941[a], wR_2 = 0.3752[b]
largest peak, hole, eÅ^{-3}	2.639, -2.261

[a] $R = \Sigma||Fo| - |Fc||/\Sigma|Fo|$. [b] $wR(F^2) = [\Sigma w(Fo^2 - Fc^2)^2/\Sigma w(Fo^2)^2]^{1/2}$ where $w = 1/[\sigma^2(Fo^2) + (0.2000P)^2]$, $P = (Fo^2 + 2Fc^2)/3$.

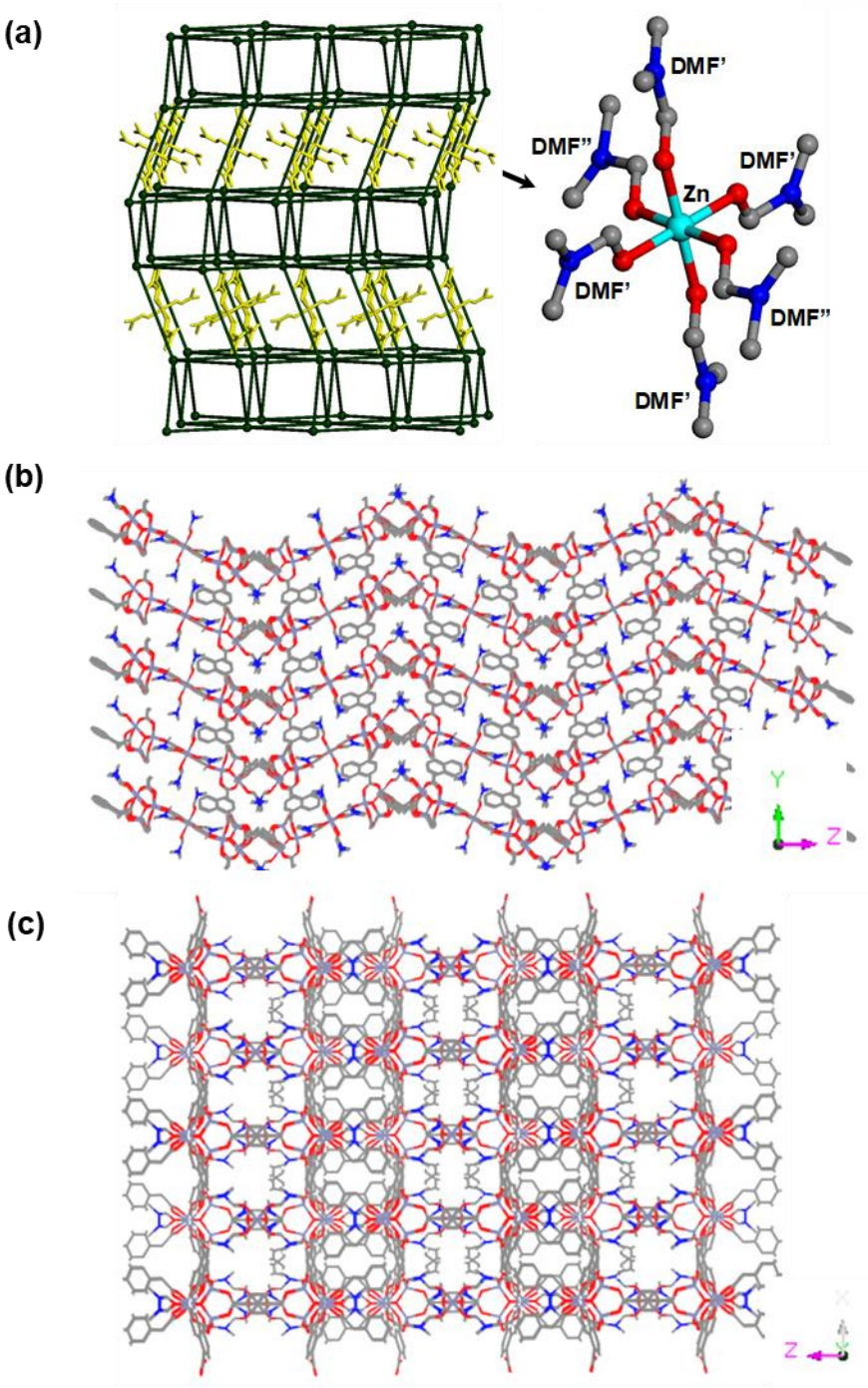

Figure 2.15 (a) The topology of 7C-MOF containing the $[Zn(DMF)_6]^{2+}$ cation complex existing in the pore of 7C-MOF and the crystal structure of 7C-MOF at (b) the YZ plane and (c) XZ plane. Disordered ndc ligands were omitted for the convenience.

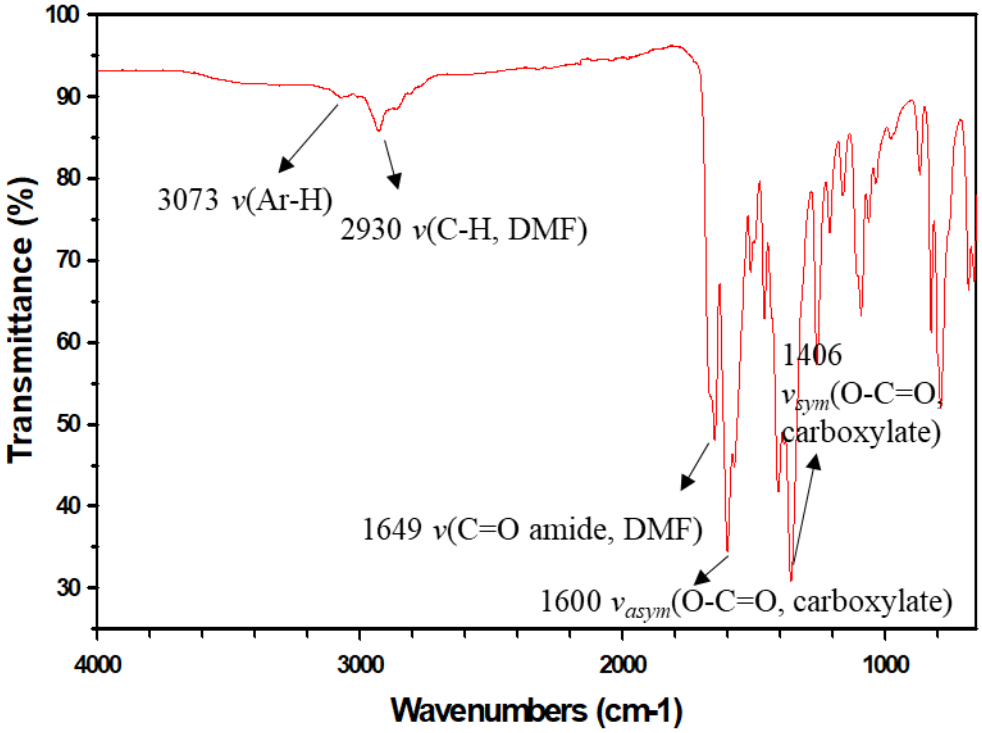

Figure 2.16 FT-IR of **7C-MOF**. Through the FT-IR data, we can indirectly verify the presence of coordinate DMF in 7C-MOF.

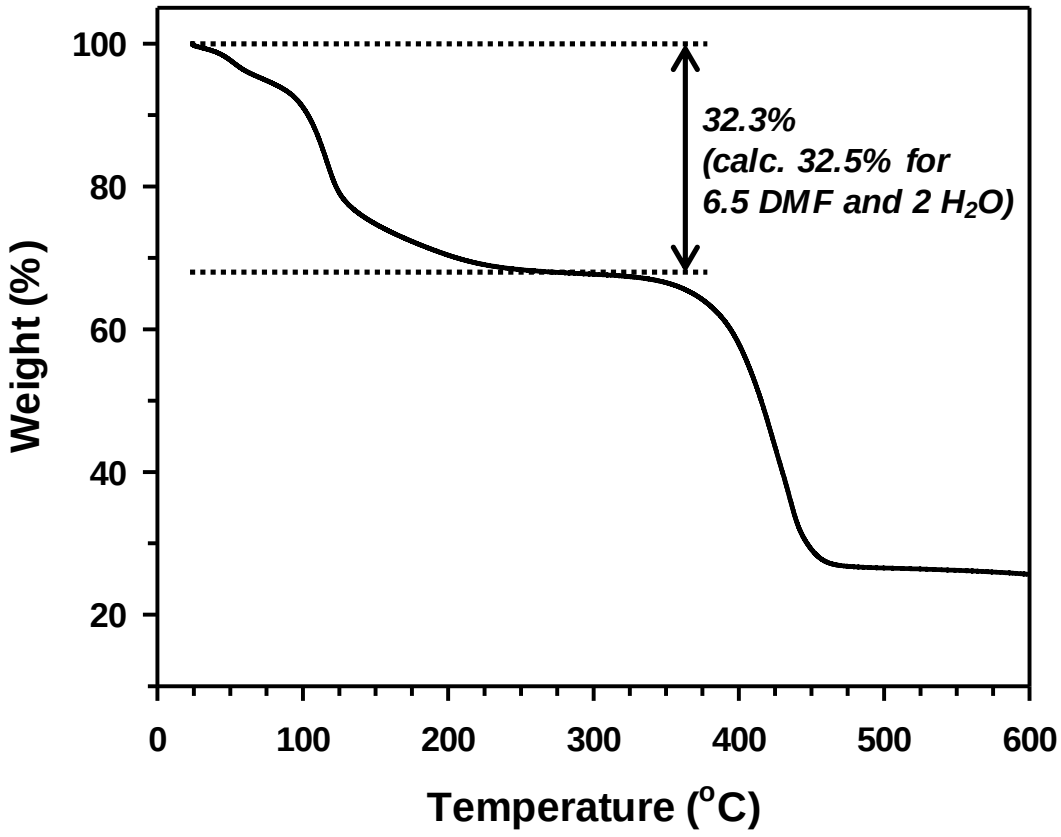

Figure 2.17 TGA trace of **7C-MOF** (5 °C per minute under N_2 atmosphere)

Table 2.2 Composition of elements (hydrogen, carbon, oxygen, and nitrogen) in 7C-MOF. Calculated represents the composition of elements that we obtained from EA of 7C-MOF. Measured represents the composition of elements that we calculated by hand based on TGA and EA.

Element	Calculated [wt. %]	Measured [wt. %]
Hydrogen	**4.64**	**4.43**
Carbon	**47.0**	**46.8**
Oxygen	**23.9**	**23.39**
Nitrogen	**6.10**	**6.05**

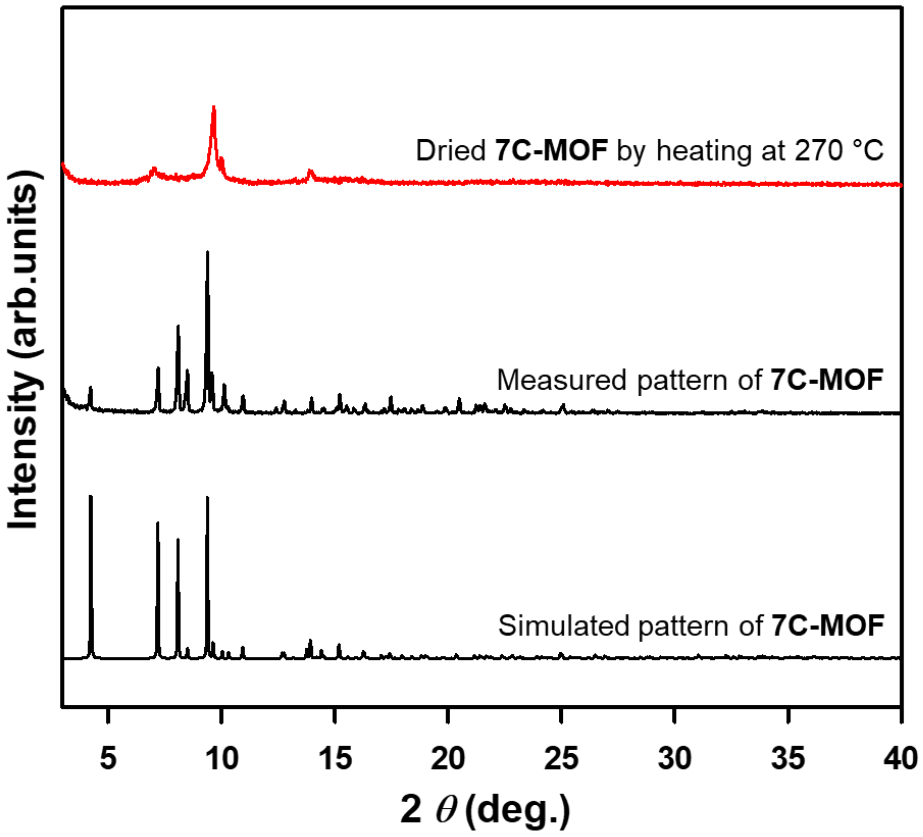

Figure 2.18 PXRD patterns of **7C-MOF** and the corresponding dried sample obtained by heating at 270 °C under vacuum for 1 h.

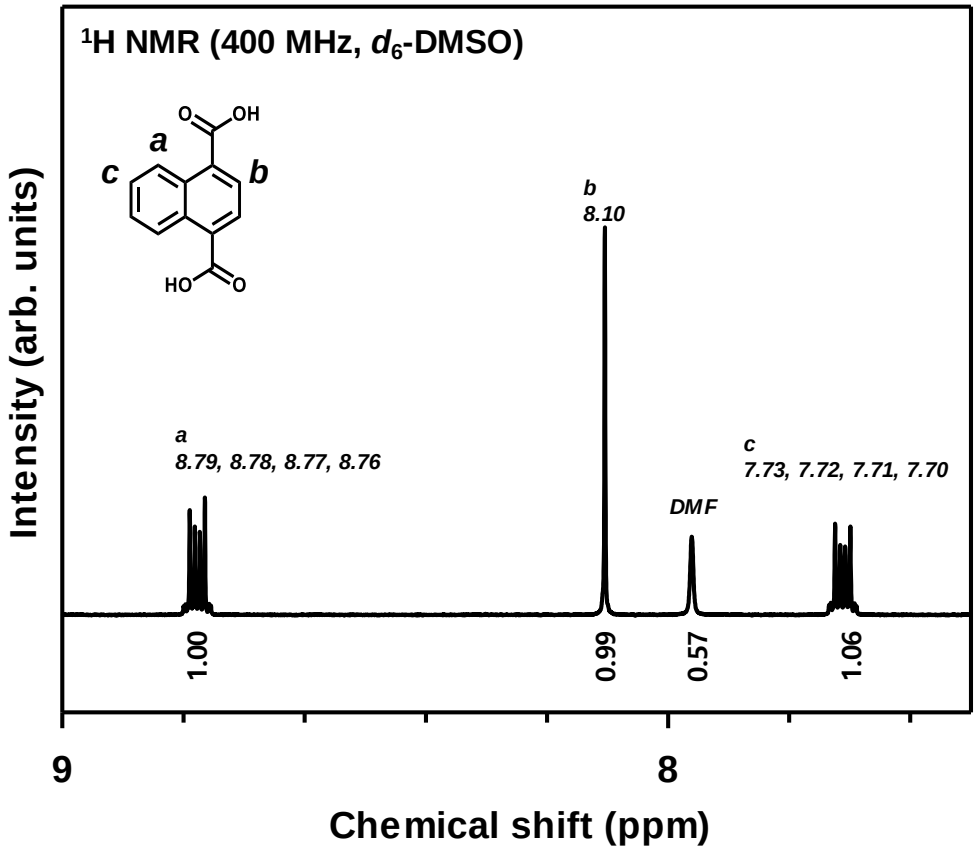

Figure 2.19 ^{1}H-NMR spectrum of **7C-MOF** after the 7C-MOF was evacuated (p is below 10^{-2} bar) at R.T. for 1.5day, prior to the gas sorption measurements. The ratio between ndc and DMF, which is estimated by integration, is in good agreement with the crystal structure that contains no free guest molecules, $\{[Zn_4(\mu_4\text{-}O)(ndc)_{3.5}(DMF)]\cdot[Zn_{0.5}(DMF)_3]\}_n$ (ndc : DMF = 3.5 : 4.0).

2.4 Conclusion

To make MOFs have specific functions for some applications, we need to synthesize a MOF with a specific crystal structure by controlling the two determinants of the crystal structures – the SBUs *per se* and/or their coordination with ligands. We investigated two main ways of synthesizing a MOF with a specific structure. We firstly conducted solid-state transformations which transform a MOF with a specific crystal structure into another MOF with another crystal structure. To explore the solid-state transformation methods, we conducted the research on the conversion of ndc-based Zn-MOFs having 6-coordinated pillared paddlewheel SBUs. Through the research, we concluded that the existence of Zn^{+}-O^{-} and weak basicity of ligands facilitates the conversion of the MOFs having pillared SBUs, resulting in another MOFs (i.e., 7C-MOF) having $Zn_4O(COO)_7$ SBUs.

3 Formation of SBUs in Synthesizing bdc-based Zn MOFs

3.1 Introduction

The crystal structures of MOFs are often randomly decided when synthesizing MOFs at once while newly creating SBUs and building their coordination with ligands. To systematically control the crystal structures of MOFs, researchers conducted research on controlling parameters to build the crystal structures of MOFs [44-52]. In case of Zr-based MOFs having tetratopic ligands, there are various crystal structures of the MOFs that are reported including **csq. ftw**, **lvt**, and **sci**, **scu, shp** topologies. One way to control the crystal structures of Zr-MOFs is to use different types of modulators. For example, a Zr-MOF having **csq** topology can be synthesized by using benzoic acid modulator [44] while a Zr-MOF having **scu** topology can be synthesized by using 4-amino-benzoic acid modulator [45].

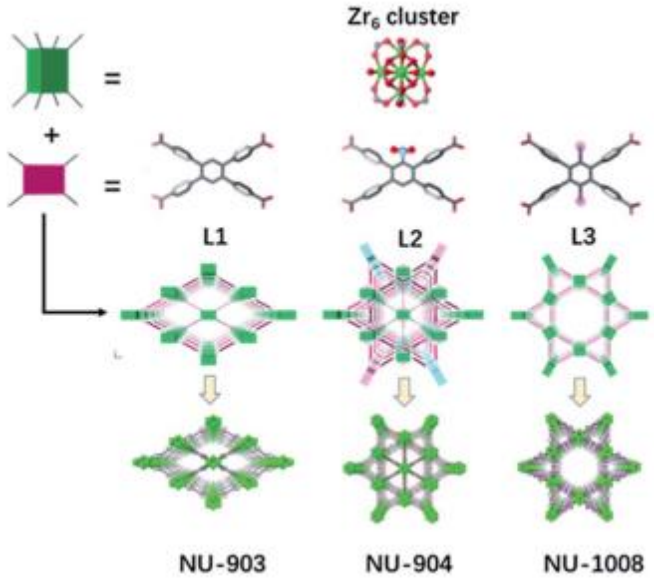

Figure 3.1 Topology control of Zr-MOFs by changing ligands [46].

Another way to control the crystal structures of Zr-MOFs is to attach different functional groups to ligands that are used to build the Zr-MOFs. For example, nitro group or bromo group were added to 1,2,4,5-tetrakis(4-carboxyphenyl) benzene ligands, resulting in the different level of bulkiness of the ligands. By the different bulkiness of the ligands, two different Zr-MOFs (i.e., NU-904 and NU-1008) were obtained (Figure 3.1) [46]. Nu-904 has **shp** topology while NU-1008 has **csq** topology.

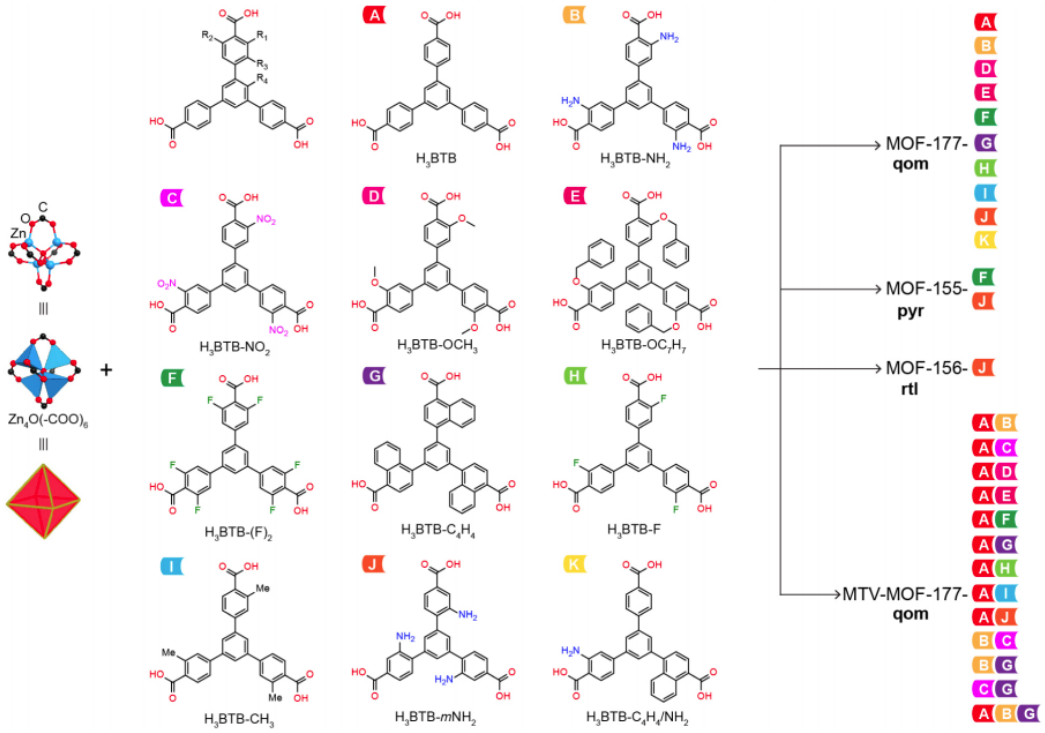

Figure 3.2 Crystal structures of MOFs having $Zn_4O(COO)_6$ SBUs and their coordination with BTB derivatives (BTB = triangular 1, 3, 5 – benzenetribenzoate) [47].

As well as the control of the crystal structures of the Zr-based MOFs, the control of the crystal structures of the Zn-based MOFs have been also controlled. Yaghi and coworkers synthesized 24 different crystal structures of MOFs having $Zn_4O(COO)_6$ SBUs and their coordination with BTB derivatives (BTB = triangular 1, 3, 5 – benzenetribenzoate) (Figure 3.2) [47]. By changing functional groups and their positions at the BTB ligands, each MOF has its own topology (i.e., **qom**, **pyr**, or **rtl** topologies). Cohen et al. obtained two different crystal structures of the Zn-based MOFs having Zn_4O SBUs and their coordination with BTB derivatives [48]. In particular by utilizing methoxy and hydroxy groups as the functional groups of the BTB ligands, they obtained a MOF having **qom** topologies and the other MOF having interpenetrated **pcu-e** topology.

To more explore the topology control of Zn-based MOFs, we studied the topology control of bdc-based Zn-MOFs (bdc = benzene-1,4-dicarboxylate) and verified impact of two parameters -reaction temperature and molar ratio of metal precursors to ligand precursors – on the determination of their own crystal structures.

Firstly, to verify that reaction temperature impacts on the determination of the crystal structures of bdc-based Zn-MOFs, we conducted the solvothermal reactions between zinc nitrate hexahydrate, which is a metal precursor, and H_2bdc, which is a ligand precursor, in a DEF solution. at each different temperature (i.e., 70, 85, 100, and 130 °C). Through the solvothermal reaction, we could successfully obtain MOF-5 having $Zn_4O(COO)_6$ SBUs at 85, 100, and 130 °C and a new MOF having $Zn_3(COO)_6$ SBUs at 70 °C.

Secondly, to verify molar ratio of metal precursors to ligand precursors affects SBUs of forming MOFs, we conducted the solvothermal reactions zinc nitrate hexahydrate, which is a metal precursor, and H_2bdc, which is a ligand precursor, in a DEF solution at the following molar ratios of precursors: (1) molar ratio of zinc nitrate hexahydrate : H_2bdc = 4:1, (2) molar ratio of zinc nitrate hexahydrate : H_2bdc = 2:1, (3) molar ratio of zinc nitrate hexahydrate : H_2bdc = 1:1, (4) molar ratio of zinc nitrate hexahydrate : H_2bdc = 1:2, (5) molar ratio of zinc nitrate hexahydrate : H_2bdc = 1:4. Trough the solvothermal reaction, we could obtain MOF-5 having $Zn_4O(COO)_6$ SBUs at 4 : 1, 2 : 1, and 1:1 molar ratios, a new MOF having $Zn_3(COO)_6$ SBUs in which DMF solvent is coordinated at 1 : 2 molar ratio, another new MOF having $Zn_3(COO)_6$ SBUs linked by bdc ligands at molar ratio of $Zn(NO_3)_2 \cdot 6H_2O$: H_2bdc = 1 : 4.

3.2 Experimentation

3.2.1 Materials and instruments The crystal structures were solved by the intrinsic phasing method with SHELX-XT (Ver. 2018/2), and refined by full-matrix least-squares calculation with SHELX-XL (Ver. 2018/3). All non-hydrogen atoms in whole structures were refined anisotropically. Although some structure solvents were observed by Fourier Mapsin the X-ray diffraction, the exact position of these solvent molecules could not be well defined due to disordered solvent of diffused electron densities. Using the SQUEEZE routine in the software of PLATON,[S5] we performed the final structure refinements.

3.2.2 Synthesis of bdc-based Zn-MOF (zinc nitrate hexahydrate: terephthalic acid = 4:1)

Zinc nitrate hexahydrate (472 mg, 1.60 mmol) and 1,4-naphthalenecarboxylic acid (0.087 g, 0.0004 mol) were added in DEF (0.01 L) in a 0.035 L glass bottle. The solution was treated at 100 °C for one day.

3.2.3 Synthesis of bdc-based Zn-MOF (zinc nitrate hexahydrate: terephthalic acid = 2:1)

Zinc nitrate hexahydrate (0.236 g, 0.0008 mol) and 1,4-naphthalenecarboxylic acid (0.087 g, 0.0004 mol) were added in DEF (0.01 L) in a 0.035 L glass bottle. The solution was treated at 100 °C for one day.

3.2.4 Synthesis of bdc-based Zn-MOF (zinc nitrate hexahydrate: terephthalic acid = 1:1)

Zinc nitrate hexahydrate (0.118 g, 0.0004 mol) and 1,4-naphthalenecarboxylic acid (0.087 g, 0.0004 mol) were added in DEF (0.01 L) in a 0.035 L glass bottle. The solution was treated at 100 °C for one day.

3.2.5 Synthesis of bdc-based Zn-MOF (zinc nitrate hexahydrate: terephthalic acid = 1:2)

Zinc nitrate hexahydrate (0.118 g, 0.0004 mol) and 1,4-naphthalenecarboxylic acid (0.174 g, 0.0008 mol) were added in DEF (0.01 L) in a 0.035 L glass bottle. The solution was treated at 100 °C for one day.

3.2.6 Synthesis of bdc-based Zn-MOF (zinc nitrate hexahydrate: terephthalic acid = 1:4)

Zinc nitrate hexahydrate (0.118 g, 0.0004 mol) and 1,4-naphthalenecarboxylic acid (0.348 g, 0.001.6 mol) were added in DEF (0.01 L) in a 0.035 L glass bottle. The solution was treated at 100 °C for one day.

3.2.7 Synthesis of bdc-based Zn-MOF (reaction temperature: 70 °C)

Zinc nitrate hexahydrate (0.118 g, 0.0004 mol) and 1,4-naphthalenecarboxylic acid (0.087 g, 0.0004 mol) were added in DEF (0.01 L) in a 0.035 L glass bottle. The solution was treated at 70 °C.

3.2.8 Synthesis of bdc-based Zn-MOF (reaction temperature: 85 °C)

Zinc nitrate hexahydrate (0.118 g, 0.0004 mol) and 1,4-naphthalenecarboxylic acid (0.087 g, 0.0004 mol) were added in DEF (0.01 L) in a 0.035 L glass bottle. The solution was treated at 85 °C.

3.2.9 Synthesis of bdc-based Zn-MOF (reaction temperature: 100 °C)

Zinc nitrate hexahydrate (0.118 g, 0.0004 mol) and 1,4-naphthalenecarboxylic acid (0.087 g, 0.0004 mol) were added in DEF (0.01 L) in a 0.035 L glass bottle. The solution was treated at 100 °C.

3.2.10 Synthesis of bdc-based Zn-MOF (reaction temperature: 130 °C)

Zinc nitrate hexahydrate (0.118 g, 0.0004 mol) and 1,4-naphthalenecarboxylic acid (0.087 g, 0.0004 mol) were added in DEF (0.01 L) in a 0.035 L glass bottle. The solution was treated at 130 °C.

3.3 Results and Discussion

Table 3.1 Secondary building units that are formed at each reaction temperature and molar ratio of metal precursors to ligand precursors.

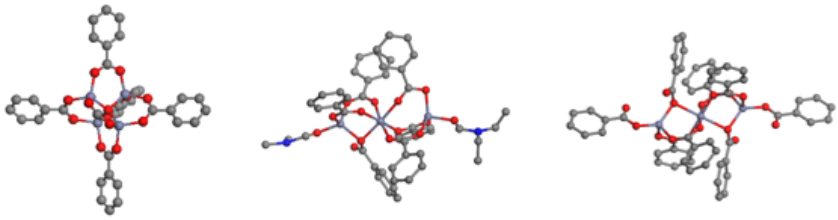

	MOF-5	COMPOUND 1	COMPOUND 2
SBU of each MOF	**$Zn_4O(COO)_6$**	**$Zn_3(COO)_6$**	**$Zn_3(COO)_6$**
Characteristics		Coordinated with terminal DMFs	Linked by bdc pillars
Reaction Temperature [ºC]	130, 100, 85 (Higher Temp.)	70 (Lower Temp.)	
Molar ratio [$Zn(NO_3)_2{\cdot}6H_2O$: H_2BDC]	4 : 1, 2 : 1, 1: 1 (Higher Molar Ratio)	1 : 2 (Lower Molar Ratio)	1 : 4 (Lower Molar Ratio)

3.3.1 Reaction temperature

While the solid-state transformation is to transform a MOF into another MOF, we wanted to obtain a MOF with a specific crystal structure at once by newly creating SBUs and building their coordination with ligands. The MOFs that we wanted to obtain were bdc-based Zn-MOFs (bdc = benzene-1,4-dicarboxylate). We figured out that the two parameters – reaction temperature and molar ratio of precursors (i.e., metal precursors and ligand precursors) – influence the determination of the crystal structures of bdc-based Zn-MOFs.

Firstly, we verified how reaction temperatures affect the determination of the crystal structures of bdc-based Zn-MOFs while the MOFs are synthesizing at once without the solid-state transformations. Zinc nitrate hexahydrate (0.4 mmol, 119 mg) and H_2bdc (0.4 mmol, 86 mg) were heated in a 10 mL DEF solution at the following temperature: (1) 70 °C, 85 °C, 100 °C, and 130 °C. Through the solvothermal reaction, we could obtain MOF-5 having $Zn_4O(COO)_6$ SBUs at 85 °C, 100 °C, and 130 °C. Interestingly, even though the phase of the MOF-5 was dominant at 85 °C , a new phase of a MOF having $Zn_3(COO)_6$ SBUs (hereinafter, COMPOUND 1) was slightly shown at a 85 °C, and the MOF having $Zn_3(COO)_6$ SBUs was dominant at 70 °C. Such information about the crystal structure of each MOF was confirmed via powder X-ray diffraction (PXRD) (Figure 3.3).

Based on our research results about reaction temperature effect on the determination of the crystal structures of the bdc-based Zn-MOFs, we concluded that we can control the crystal structure of the bdc-based Zn-MOFs while synthesizing the MOFs at once by varying reaction temperature. Here, we would say that COMPOUND 1 having $Zn_3(COO)_6$ SBUs that was formed at at 70 °C is a kinetic bdc-based Zn-MOF while MOF-5 having $Zn_4O(COO)_6$ SBUs that was formed at 85 °C, 100 °C, and 130 °C is a thermodynamic bdc-based Zn-MOF.

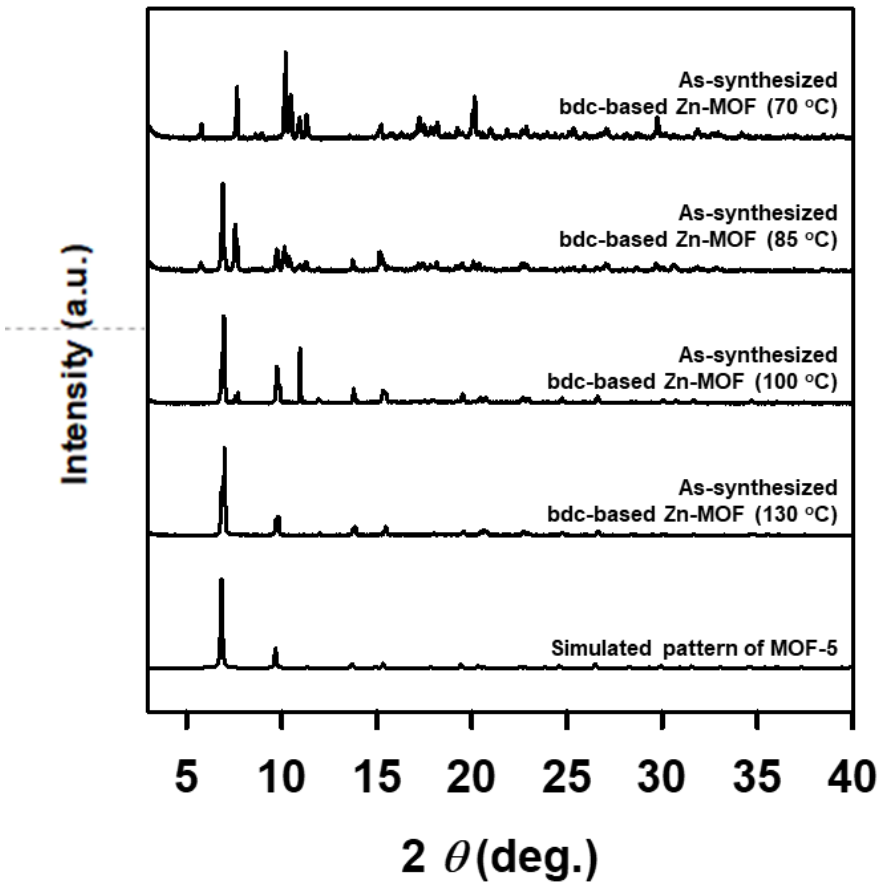

Figure 3.3 PXRD patterns of bdc-based Zn-MOFs after the solvothermal reaction in DEF at each reaction temperature 70, 85, 100, and 130 °C. During the solvothermal reaction, the new phase of a MOF having $[Zn_3(\text{-}COO)_6]$ SBUs was started to be shown at 85 °C and the new phase is dominant at 70 °C (COMPOUND 1).

3.3.2 Molar ratio of metal precursors to ligand precursors

Secondly, we verified how molar ratio of metal precursors to ligand precursors affects the final crystal structures of bdc-based Zn-MOFs while the MOFs are synthesizing at once without the solid-state transformations. $Zn(NO_3)_2 \cdot 6H_2O$ and H_2bdc (benzne-1,4-dicarboxylic acid) were heated in a 10 mL DEF solution at 100 °C for 24 hours. The molar ratios of $Zn(NO_3)_2 \cdot 6H_2O$ to H_2bdc were varied like the following condition: molar ratio of $Zn(NO_3)_2 \cdot 6H_2O$: H_2bdc = 4 : 1, 2 : 1, 1 : 1, 1 : 2, and 1 : 4.

Through the solvothermal reaction, we could obtain MOF-5 having $Zn_4O(COO)_6$ SBUs in the following condition: $Zn(NO_3)_2 \cdot 6H_2O$: H_2bdc = 4 : 1, 2 : 1, and 1 : 1. Interestingly, in the condition $Zn(NO_3)_2 \cdot 6H_2O$: H_2bdc = 1 : 2, 1 : 4, we could obtain two different MOFs having $Zn_3(COO)_6$ SBUs, which were analyzed by powder X-ray diffraction (PXRD) (Figure 3. 4). The crystal structures of the two different MOFs that we obtained in the condition $Zn(NO_3)_2 \cdot 6H_2O$: H_2bdc = 1 : 2, 1 : 4 were also verified using SCXRD (Figures 3.5 and Figure 3.6).

In case of a Zn-MOF (i.e., COMPOUND 1) that was formed in the condition $Zn(NO_3)_2 \cdot 6H_2O$: H_2bdc = 1 : 2 (Figure 3.5), the crystal structure is built by $Zn_3(COO)_6$ SBUs and shows two-dimensional structure. The Zn^{2+} based SBUs are coordinated with six bdc^{2-} ligands and two terminal Zn^{2+} nodes are coordinated with two terminal DMF molecules. In the secondary building unit, 2 Zinc ions existed in 4 connected tetragonal structures, while the other zinc ions exist in a six-connected octahedral structure. The same crystal structure was already reported by other research groups [53-54]. Lee group reported the identical topology of the MOF where Zn^{2+} based SBUs are coordinated with six bdc^{2-} ligands but two terminal ethanol molecules instead of DMF molecules were coordinated to each SBU [53]. Walton and coworkers also reported the same structure of the MOF, in which water molecules instead of DMF molecules were coordinated to each SBU [54]. They have the same 3^6 topologies.

In case of the bdc-based Zn-MOF (i.e., COMPOUND 2) that was formed formed in the condition $Zn(NO_3)_2 \cdot 6H_2O$: H_2bdc = 1 : 4 (Figure 3.6), the crystal structure is built by $Zn_3(COO)_6$ SBUs and shows three-dimensional structure. The Zn^{2+} based SBUs are coordinated with six bdc^{2-} ligands and bdc pillars link the bdc-linked planed, resulting in three-dimensional structure. In the secondary building units, 2 zinc ions existed in 4 connected tetragonal structures, while the other Zn ions exist in a six-connected octahedral structures. In particular, when we solved the crystal structure of the MOF using SCXRD, the charge imbalance of the 6-coordinated SBU was considered due to the bdc pillars or, pillar bdc presumably was not deprotonated to compensate the charge imbalance.

Based on our research results about molar ratio of metal precursors to ligand precursors impact on the determination of the crystal structures of the bdc-based Zn-MOFs, we concluded that we can control the crystal structure of the bdc-based Zn-MOFs while synthesizing the MOFs at once by varying molar ratio of metal precursors to ligand precursors. Here, we would say that trends of creating a MOF with certain crystal structure in this molar ratio effect is proportional to the temperature effect as we discussed **in section 3.3.1**

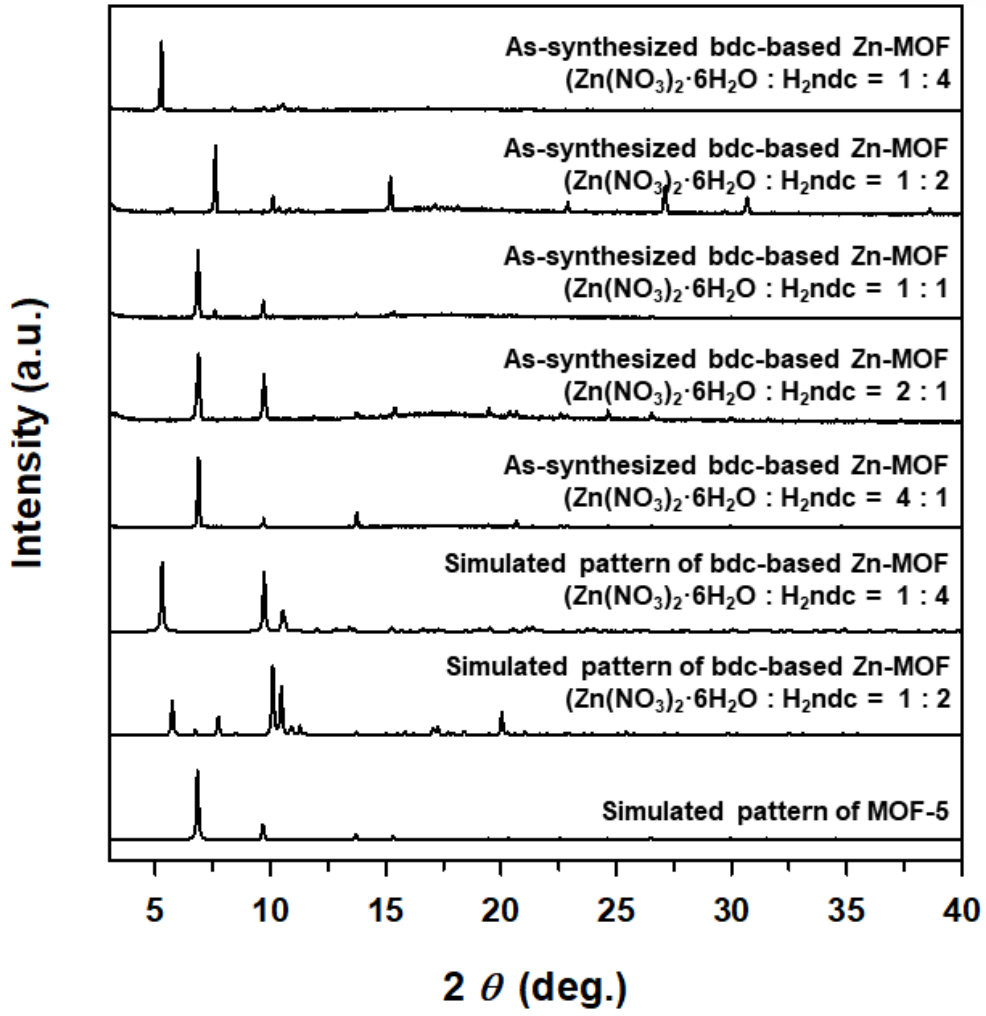

Figure 3.4 PXRD patterns of bdc-based Zn-MOFs before and after the solvothermal reaction in DEF at 100 °C for 24 h at each molar ratio of metal to ligand precursors (i.e., molar ratio of $Zn(NO_3)_2 \cdot 6H_2O$: H_2bdc = 4 : 1, 2 : 1, 1 : 1, 1 : 2, and 1 : 4). During the solvothermal reaction, the new phase of MOFS is shown at molar ratio of $Zn(NO_3)_2 \cdot 6H_2O$: H_2bdc = 1 : 2 and 1 : 4. In case of 1 : 2 molar ratio, a MOF having $Zn_3(COO)_6$ SBUs at which DMF solvent is coordinated was obtained while a MOF having $Zn_3(COO)_6$ SBUs linked by bdc (benzne-1,4-dicarboxylate) was obtained at 1 : 4 molar ratio.

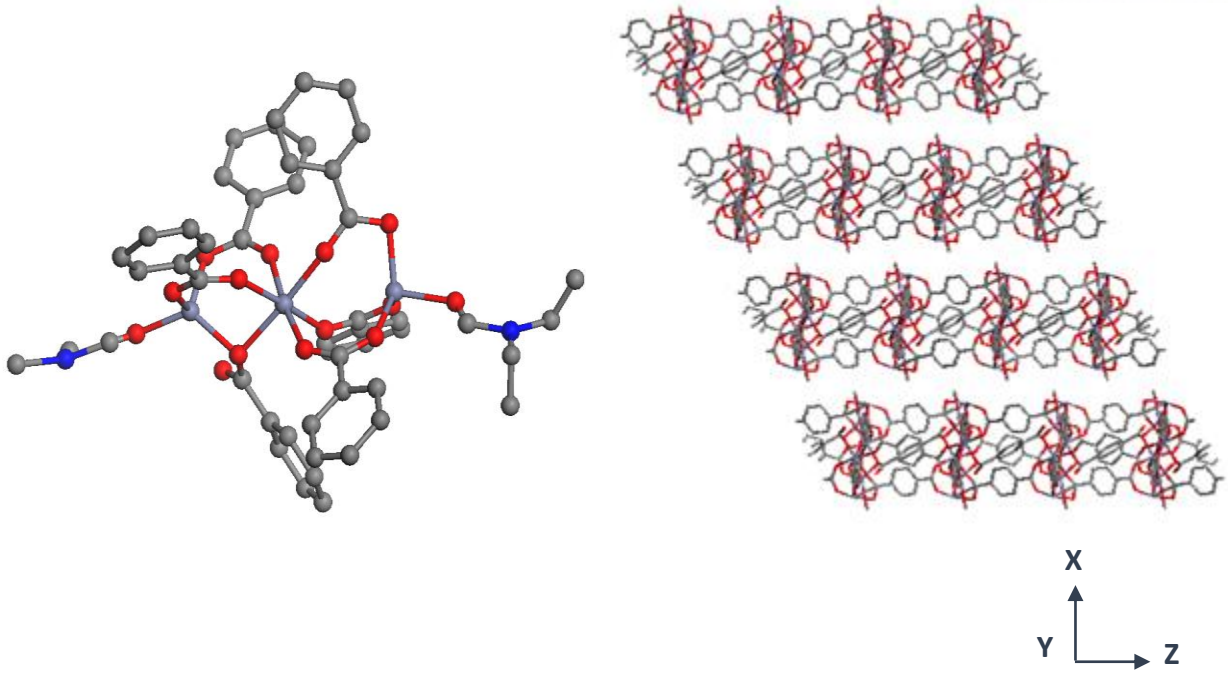

Figure 3.5 Crystal structure of the bdc-based Zn-MOF that was obtained in the condition: molar ratio of $Zn(NO_3)_2 \cdot 6H_2O$: H_2bdc = 1: 2(COMPOUND 1). a = 25.083(5), b = 20.806(4), c = 17.748(4), alpha = 90, beta = 114.39(3), gamma = 90. The crystal structure consists of $[Zn_3(\text{-}COO)_6]$ SBUs at which DMF solvent is coordinated (left side) and forms two-dimensional structure (right side). Please note that the coordinated DMF molecules are omitted to clearly show the two-dimensional stacking in the right side

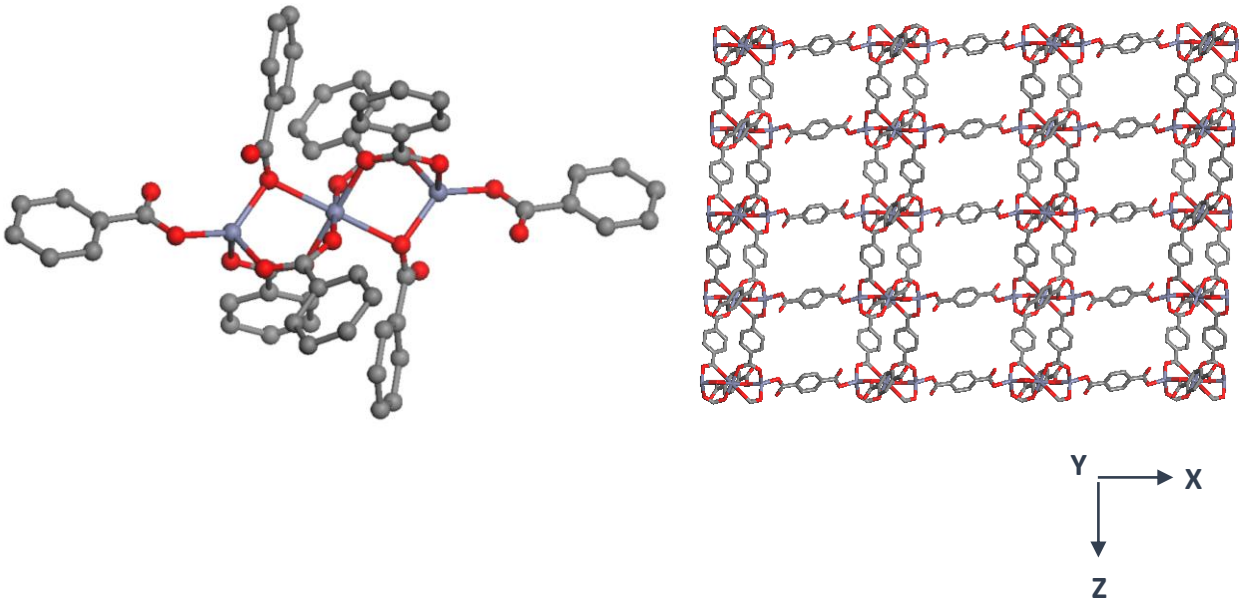

Figure 3.6 Crystal structure of the bdc-based Zn-MOF that was obtained in the condition: molar ratio of $Zn(NO_3)_2 \cdot 6H_2O$: H_2bdc = 1: 4 (COMPOUND 2). a = 33.382(7), b = 9.824(2), c = 18.193(4), alpha = 90, beta = 92.48(3), gamma = 90. The crystal structure consists of $[Zn_3(\text{-}COO)_6]$ SBUs linked by bdc (benzne-1,4-dicarboxylate) and forms three-dimensional structure.

3.4 Conclusion

In the section 3 Topology Control of MOFs, we conducted the topology control of bdc-based Zn-MOFs depending on reaction temperature and molar ratio of metal precursors to ligand precursors. In the research on reaction temperature effect, we could successfully obtain MOF-5 having $Zn_4O(COO)_6$ SBUs at 85, 100, and 130 °C reaction temperatures and a MOF having $Zn_3(COO)_6$ SBUs at 70 °C reaction temperature. In the research on molar ratio of precursors (i.e., zinc nitrate hexahydrate : H_2ndc) effect, we could obtain MOF-5 having $Zn_4O(COO)_6$ SBUs in the following condition: molar ratio of $Zn(NO_3)_2 \cdot 6H_2O$: H_2bdc = 4 : 1, 2 : 1, and 1 : 1. Another Zn-MOF having $Zn_3(COO)_6$ SBUs in which two terminal DMF molecules are coordinated was obtained in the molar ratio of $Zn(NO_3)_2 \cdot 6H_2O$: H_2bdc = 1 : 2 while the other Zn- MOF having $Zn_3(COO)_6$ SBUs linked by bdc pillars in the molar ratio of $Zn(NO_3)_2 \cdot 6H_2O$: H_2bdc = 1 : 4. Based on our research results about reaction temperature and molar ratio of metal to ligand precursors effect on the determination of the crystal structures of the bdc-based Zn-MOFs, we concluded that a MOF having $Zn_3(COO)_6$ SBUs that was formed at at 70 °C is a kinetic bdc-based Zn-MOF while MOF-5 having $Zn_4O(COO)_6$ SBUs that was formed at 85 °C, 100 °C, and 130 °C is a thermodynamic bdc-based Zn-MOF. Also, we would say that trends of creating a MOF with certain crystal structure in this molar ratio effect is proportional to the temperature effect.

4 CO_2 Cycloaddition of 7C-MOF

4.1 Introduction

CO_2 emission is one of the main causes to trigger global warming all around the world. Thus, it is important to deal with the increasing amount of the CO_2 emission. CO_2 conversion reactions have been promising solutions to deal with the issue because through the reactions, CO_2 is converted into valuable chemicals including C1 feedstocks. Among various CO_2 conversion reactions, CO_2 cycloaddition is the reaction in which epoxide and CO_2 react with each other and produce cyclic carbonate (Figure 4.1). The resulting cyclic carbonate can be used in many applications including electrolyte solvents and biomedical products [55-57].

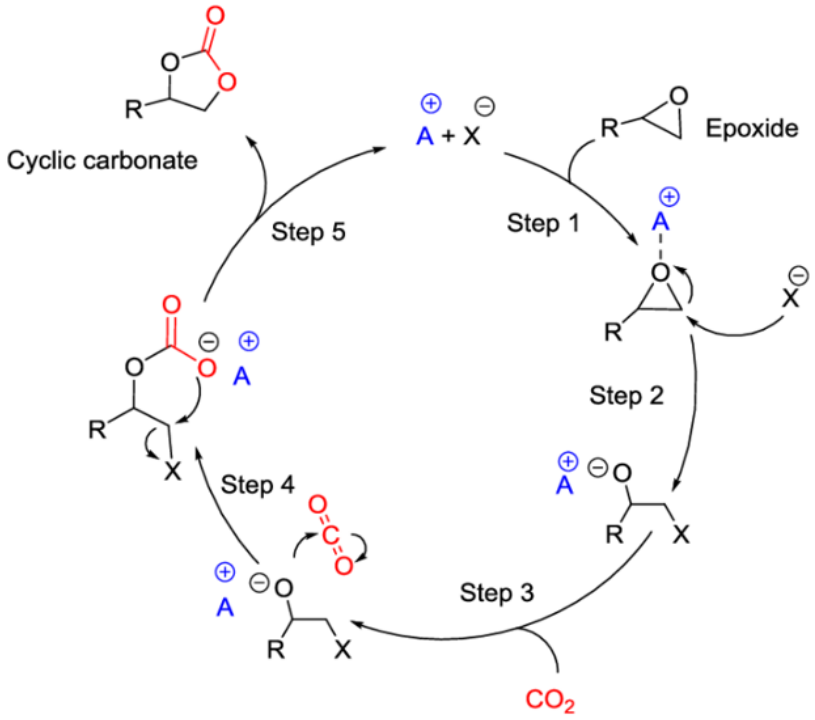

Figure 4.1 Schematic catalytic mechanism for CO_2 cycloaddition [70].

MOFs are promising heterogeneous catalysts due to structural diversity as we described **in section 1.1.** Thus, many researchers have researched MOFs-based catalysts for CO_2 cycloaddition. For example, Indium based MOFs having trinuclear and mononuclear Indium clusters showed enhanced catalytic activity because Indium metals have accessible p-orbitals and thus, the metal-based MOFs easily accept electrons, which is important to catalyze CO_2 cycloaddition (Figure 4.2) [58]. The other MOF that was constructed by octcarboxylate ligands and Cu (II) ions shows high interaction with CO_2. This characteristic creates the corresponding catalytic activity for CO_2 cycloaddition [59]. And Zn-based MOFs were also used to catalyze the CO_2 cycloaddition (Table 4.1 and Figure 4.3) [60-65].

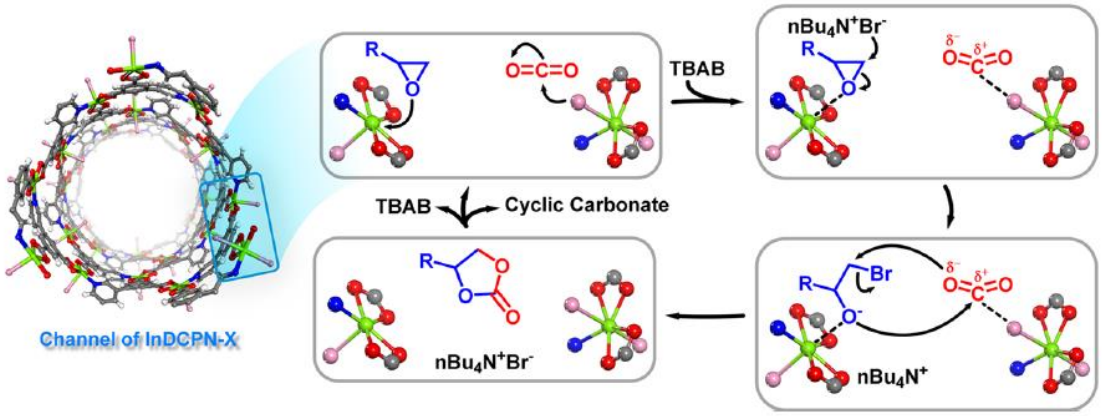

Figure 4.2 Schematic catalytic mechanism of the In-organic frameworks for CO_2 cycloaddition. Epoxide is catalyzed by an Indium based MOF. Two different types of Indium metal clusters have different function in the CO_2 cycloaddition [58].

Table 4.1 The representative Zn-based MOFs that shows the catalytic activity for CO_2 cycloaddition.

MOF	Chemical formula	Co-catalyst	Temp. (K)	CO_2 (atm)	Time (h)	Yield (%)
MOF-5	$(Zn_4O)(BDC)_3$	n-Bu_4NBr	323	60	4	98
ZnGlu	ZnGlu	n-Bu_4NBr	353	12	6	>99
UMCM-1-NH_2	$(Zn_4O)_9$(BDC-$NH_2)_6(BTB)_5$	n-Bu_4NBr	r.t.	12	24	90
$(Zn_4O)_2(Zn_2)_{1.5}$(CPD)$_6$	$(Zn_4O)_2(Zn_2)_{1.5}(CPD)_6$		r.t.	12	60	99
MMPF-18	$Zn_4(u_4\text{-}O)$(Zn-BCPP)$_3$	n-Bu_4NBr	r.t.	1	48	97
$Zn_3(PTB)_2$	$Zn_3(PTB)_2$	n-Bu_4NBr	r.t.			92
ZnGlu	ZnGlu	n-Bu_4NBr	r.t.	10	24	65

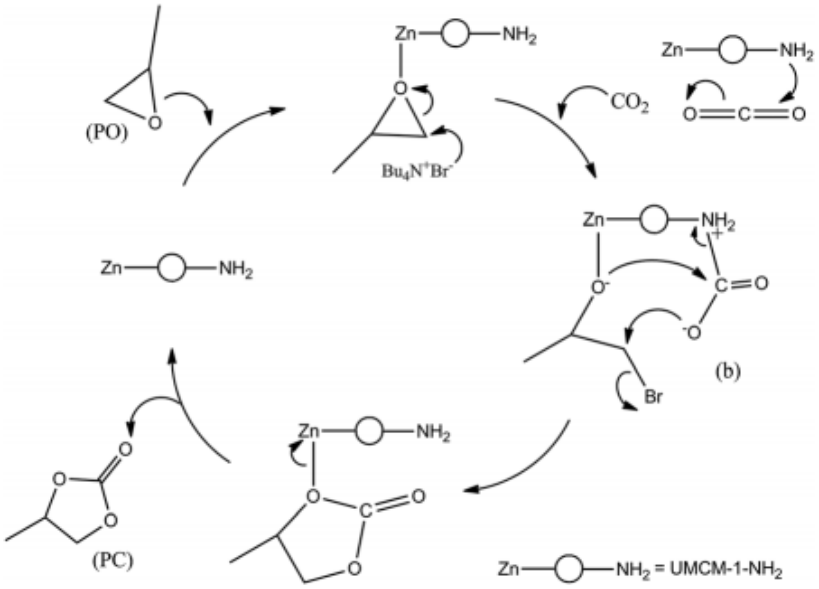

Figure 4.3 Schematic catalytic mechanism for CO_2 cycloaddition with Zn-based MOF [61].

We explored the possibility of using the 7C-MOF into the CO_2 cycloaddition. 7C-MOF has been rarely reported in the academic field, so exploring whether the MOF can be applicable into the CO_2 cycloaddition may contribute to expanding the usage of 7C-MOF. We firstly analyzed 7C-MOF's interaction with CO_2 using CO_2 sorption isotherm and found that 7C-MOF is capable of adsorbing CO_2 molecules because 7C-MOF is an anionic framework and has cation complex $[Zn(DMF)_6]^{2+}$ in the pores (Figure 2.15 (a)). By analyzing product yields (100[mole of cyclic carbonate] / [mole of cyclic carbonate and epoxide]) using H-nuclear magnetic resonance spectroscopy, we found that 7C-MOF can facilitate CO_2 cycloaddition.

4.2 Experimentation

4.2.1 Materials and instruments

All chemicals and solvents were of reagent grade and were used as received without further purification. NMR spectra were recorded on Agilent 400-MR DD2 spectrometer.

4.2.2 CO_2 cycloaddition (Condition: 0.1 mmol TBAB without 7C-MOF)

Tetrabutylammonium bromide (TBAB) (0.1 mmol, 32 mg), which is a co-catalyst was added to an autoclave batch reactor with stirring bar. After evacuating air within the reactor, propylene oxide (10 mmol, 0.6761 mL) was added and then, the reactor was filled with CO_2 (10 bar). CO_2 cycloaddition went on at room temperature for 24 h,

4.2.3 CO_2 cycloaddition (Condition: 0.1 mmol TBAB with 7C-MOF)

TBAB (0.1 mmol, 32 mg) and 7C-MOF (0.01 mmol, 13 mg) were added to an autoclave batch reactor with stirring bar. After evacuating air within the reactor, propylene oxide (10 mmol, 0.6761 mL) was added and then, the reactor was filled with CO_2 (10 bar). CO_2 cycloaddition went on at room temperature for 24 h,

4.2.4 CO_2 cycloaddition (Condition: 1 mmol TBAB with 7C-MOF)

TBAB (1 mmol, 320 mg) and 7C-MOF (0.01 mmol, 13 mg) were added to an autoclave batch reactor with stirring bar. After evacuating air within the reactor, propylene oxide (10 mmol, 0.6761 mL) was added and then, the reactor was filled with CO_2 (10 bar). CO_2 cycloaddition went on at room temperature for 24 h,

4.3 Results and Discussion

CO_2 emission is one leading cause to exacerbate global warming all around the world. Thus, it is pivotal to mitigate the increasing amount of CO_2 emission. CO_2 converting reactions are promising alternatives to deal with the issue. Through the reactions, CO_2 is converted into useful chemicals including C1 feedstocks. Among various CO_2 conversion reactions, CO_2 cycloaddition is the reaction where epoxide and CO_2 react with each other and produce cyclic carbonate (Figure 4.4). The cyclic carbonate can be used in many applications including electrolyte solvents and biomedical products. In this context, after studying how to adjust parameters to determine the crystal structures of MOFs and synthesizing the MOFs, we further explored the possibility of using a MOF synthesized by a solid-state transformation (i.e., 7C-MOF) into CO_2 cycloaddition. There are only a few researches that reported a MOF having 7-coordinated zinc-based SBUs and **sev** topology in the academic field. Thus, it is valuable to explore the catalytic activity of this MOF for CO_2 cycloaddition and then, contribute to expanding the usage of 7C-MOF.

We firstly analyzed the interaction of 7C-MOF with N_2 and CO_2 using N_2 and CO_2 sorption isotherm. While the 7C-MOF showed no porosity, which was verified by N_2 sorption isotherm (Figure 4.5 (a)), 7C-MOF showed the interaction with CO_2 gas, which was verified by N_2 sorption isotherm (i.e., max. 0.00143 mol/g of carbon dioxide adsorbed at 196 K in one stepwise way) (Figure 4.5 (a)) with no influencing the phase, which was verified by the PXRD patterns before and after the gas sorption experiment (Figure 4.5 (b)). We considered that such interaction of 7C-MOF with CO_2 molecules might results from an electrostatic field formed by the anionic framework and cation complex of $[Zn(DMF)_6]^{2+}$ in the pore [66, 67]. Regarding this characteristic of 7C-MOF, we expected that CO_2 can access to 7C-MOF and undergo CO_2 cycloaddition in which 7C-MOF act as a Lewis acid catalyst. Then, we conducted CO_2 cycloaddition like the following procedure. Tetrabutylammonium bromide (TBAB) (0.1 mmol, 32 mg), which is a co-catalyst and 7C-MOF (0.01 mmol, 13 mg) were added to an autoclave batch reactor with stirring bar. After evacuating air within the reactor, propylene oxide (10 mmol, 0.6761 mL) was added and then, the reactor was filled with CO_2 (10 bar). CO_2 cycloaddition went on at room temperature for 24 h, After finishing the reaction, product yield (100[mole of cyclic carbonate] / [mole of cyclic carbonate and epoxide])) was analyzed using H-nuclear magnetic resonance spectroscopy (^{1}H-NMR). The product yield was about 63 % (Figure 4.7). The maintenance of the structure of 7C-MOF after the CO_2 cycloaddition was confirmed using PXRD (Figure 4.8). The reference catalytic reaction, in which there was not 7C-MOF catalyst was also conducted and the product yield was about 11 % (Figure 4.6). In order to increase product yield, we increased the amount of TBAB to 1 mmol (320 mg). Even though the product yield was about 93 % (Figure 4.9) under the condition, the structure of 7C-MOF was collapsed after the CO_2 cycloaddition,

as confirmed by PXRD (Figure 4.10)

Even though we did not achieve the enhancement of the product yield to over 90 % with the maintenance of the crystal structure of the 7C-MOF, we considered one possible catalytic reaction mechanisms for the reaction, in which the product yield was 63 %. The mechanism is that two 4-coordinated zinc metal sites within the framework of 7C-MOF act as Lewis acidic sites and activate the propylene oxide to make cyclic carbonate. Even though the two zinc metal sites are not open-metal sites, they can act as Lewis acidic sites. This mechanism was considered based on previous literature that MOF-5 having 4-coordinated zinc metal sites has catalytic activity for CO_2 cycloaddition [68-69].

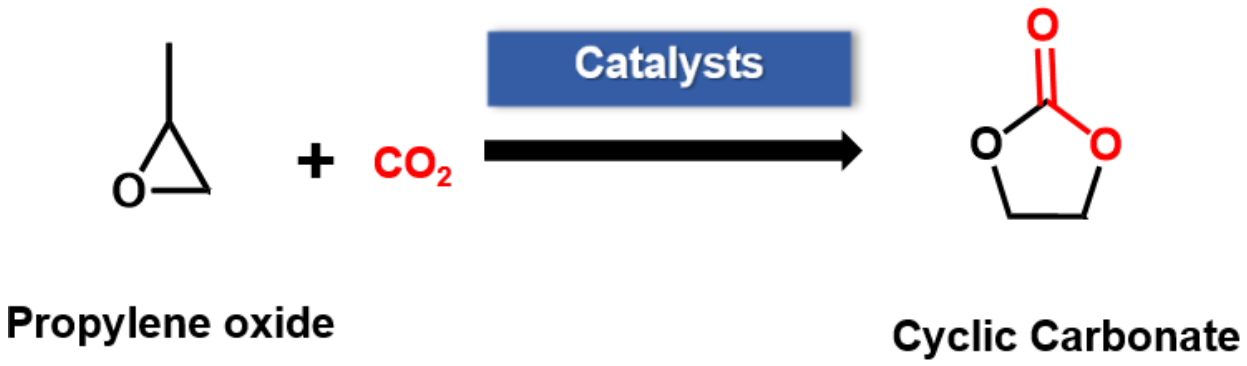

Figure 4.4 Reaction scheme of CO_2 cycloaddition, in which CO_2 reacts with epoxide to produce cyclic carbonate.

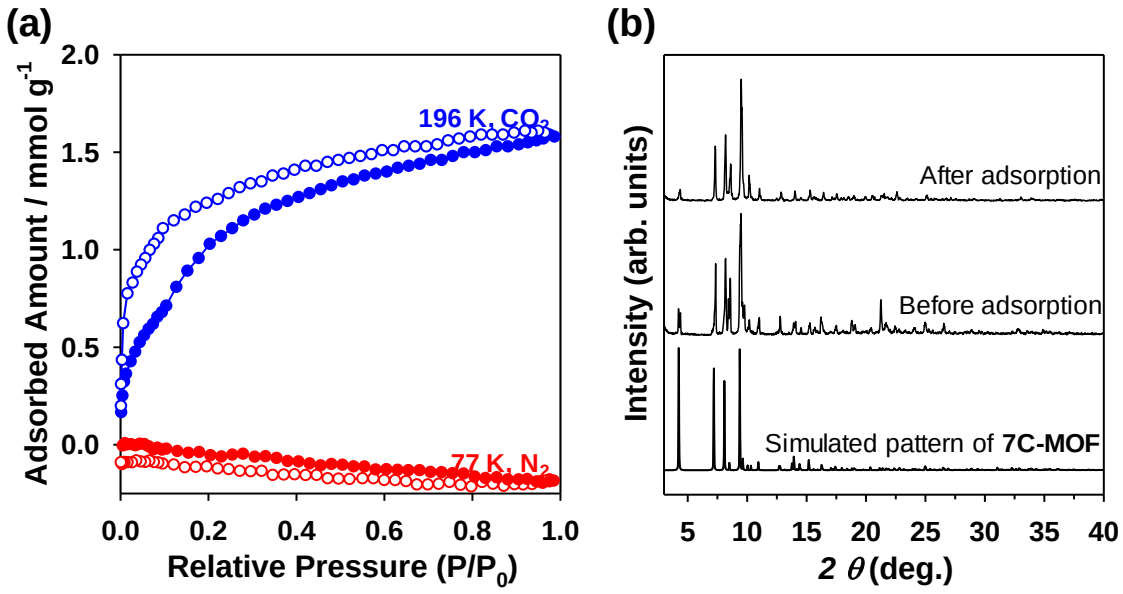

Figure 4.5 Reaction scheme of CO_2 cycloaddition with epoxide (b) PXRD patterns of 7C-MOF before and after the CO2 sorption experiment.

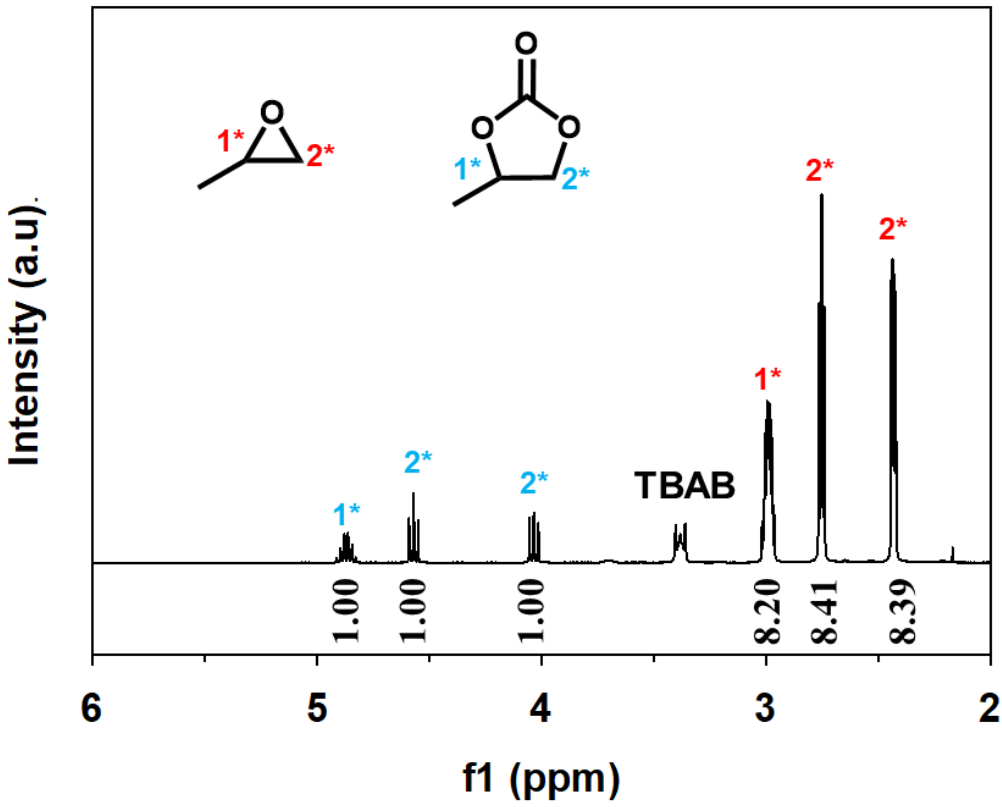

Figure 4.6 ^{1}H-NMR after CO_2 cycloaddition in the absence of 7C-MOF as a Lewis catalyst (TBAB: 0.1 mmol). The product (cyclic carbonate) yield is about 11 %.

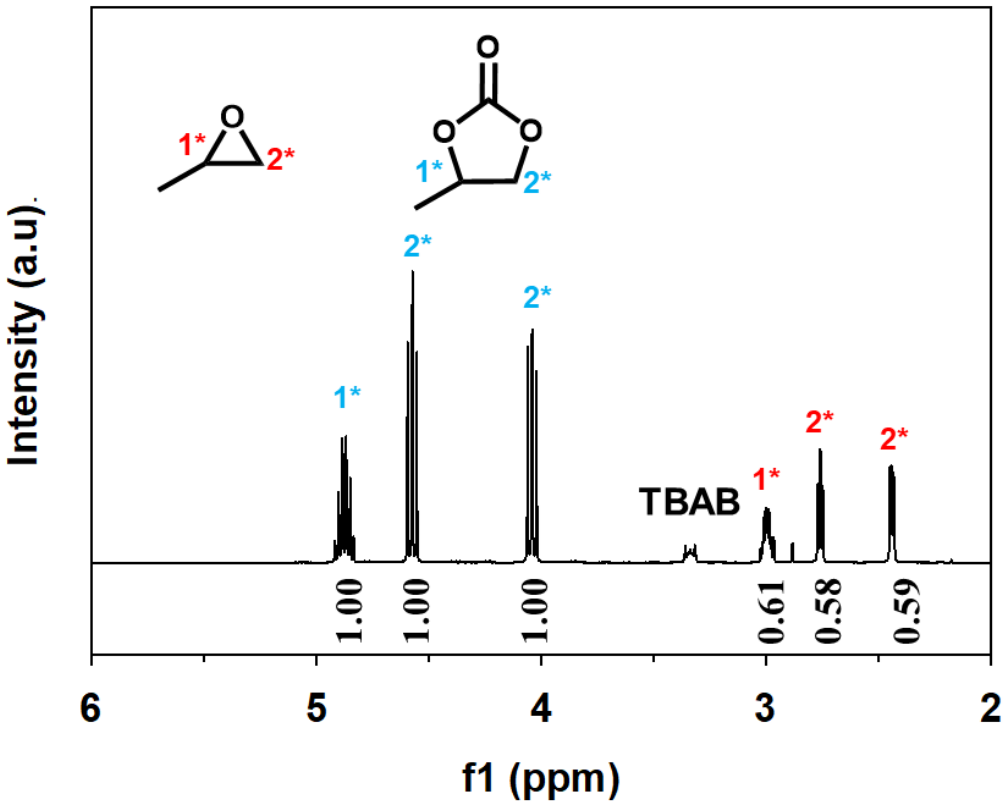

Figure 4.7 ^{1}H-NMR after CO_2 cycloaddition in the presence of 7C-MOF as a Lewis catalyst (TBAB: 0.1 mmol). The product (cyclic carbonate) yield is about 63 %.

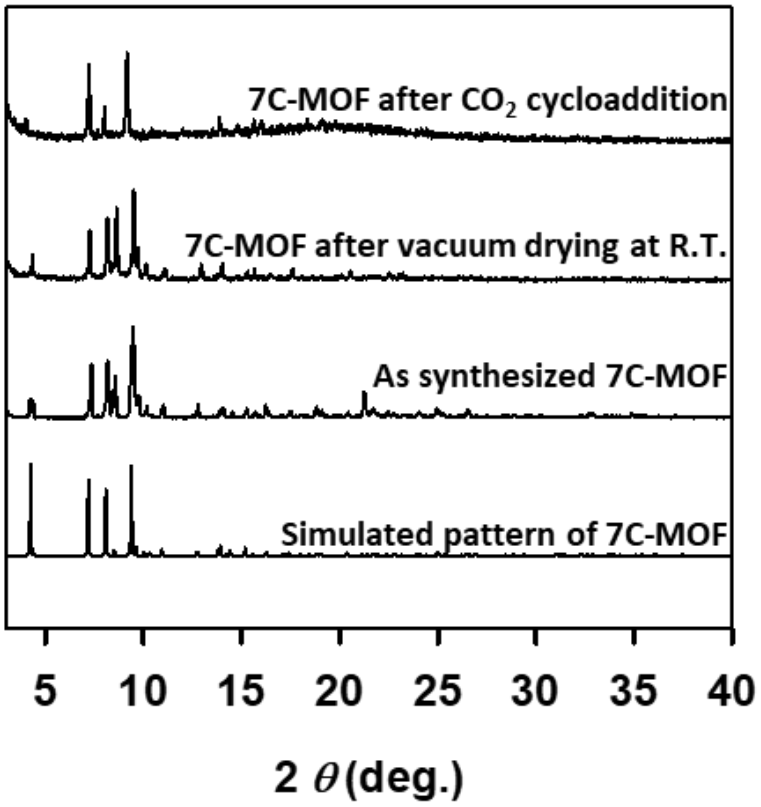

Figure 4.8 The PXRD patterns of 7C-MOF as synthesized, after vacuum drying, and after CO_2 cycloaddition (Condition: TBAB 0.1 mmol). We verified that 7C-MOF maintained its structure after the CO_2 cycloaddition.

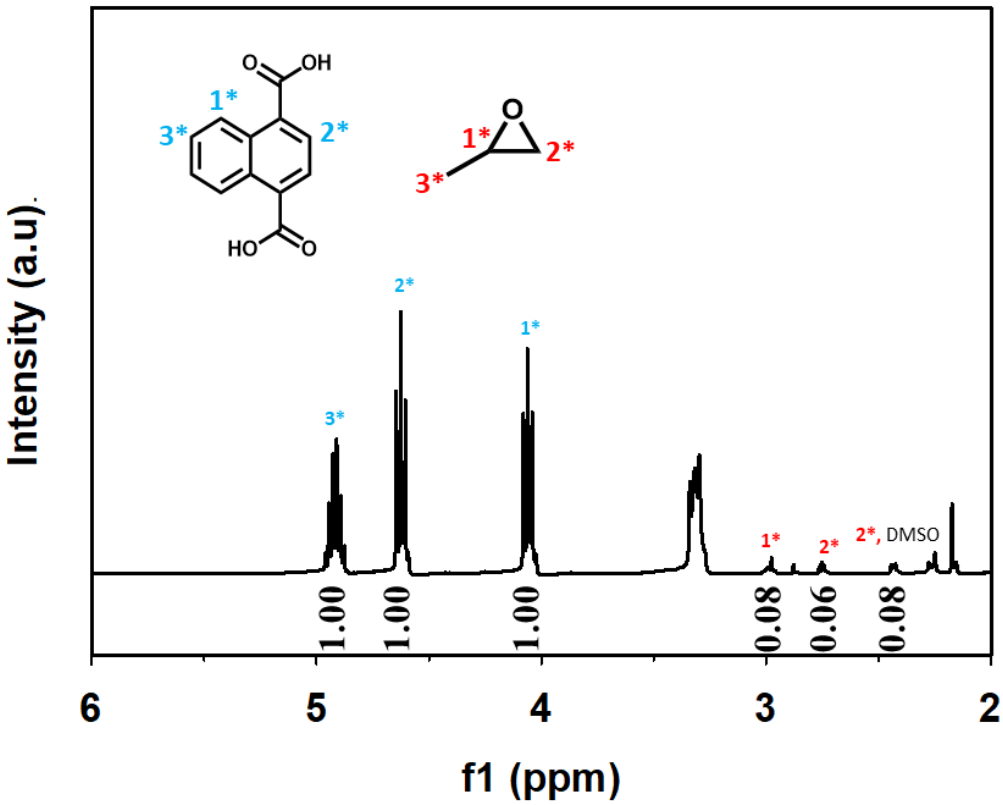

Figure 4.9 ^{1}H-NMR after CO_2 cycloaddition in the presence of 7C-MOF as a Lewis catalyst (TBAB: 1 mmol). The product (cyclic carbonate) yield is about 93 %.

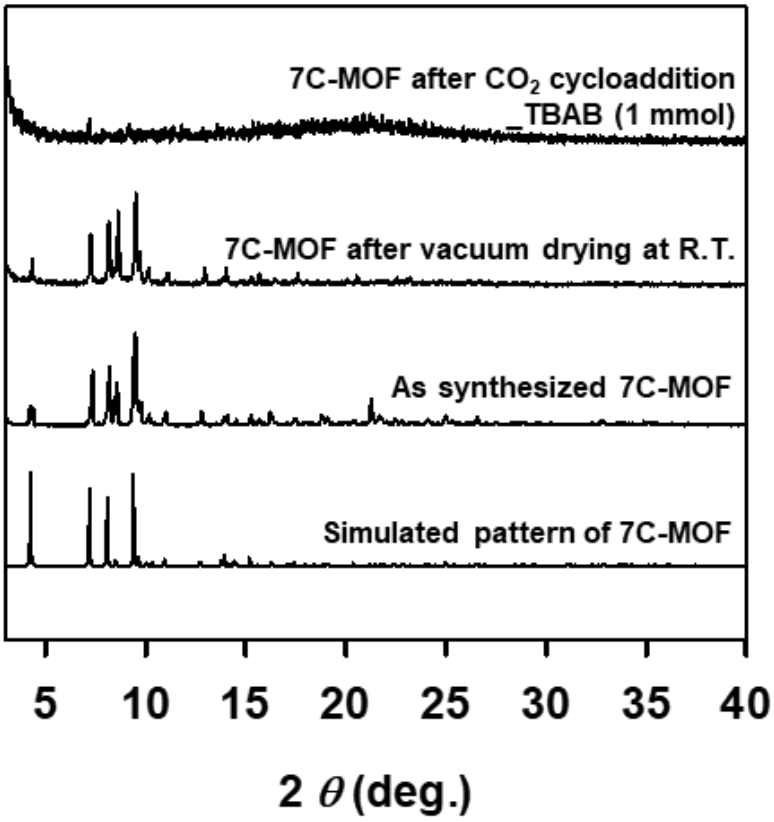

Figure 4.10 The PXRD patterns of 7C-MOF as synthesized, after vacuum drying, and after CO_2 cycloaddition (Condition: TBAB 1 mmol). We verified that the crystal structure of 7C-MOF was collapsed after the CO_2 cycloaddition.

4.5 Conclusion

We further explored the possibility of using 7C-MOF for CO_2 cycloaddition. We analyzed 7C-MOF using CO_2 sorption isotherm and found that 7C-MOF is capable of adsorbing CO_2 molecules. This is because 7C-MOF is an anionic framework and has cation complex of $[Zn(DMF)_6]^{2+}$ in its pores. Thus, we expected that 7C-MOF can act as a Lewis catalyst for CO_2 cycloaddition. By analyzing product yields (100[mole of cyclic carbonate] / [mole of cyclic carbonate and epoxide]) using H-nuclear magnetic resonance spectroscopy, we found that 7C-MOF can act as a Lewis acid catalyst which facilitates CO_2 cycloaddition.

References

[1] Mason, J. A., Veenstra, M., & Long, J. R. Evaluating metal–organic frameworks for natural gas storage. *Chem Sci.* 2014, 5, 32–51.

[2] Bachman, J. E., Kapelewski, M. T., Reed, D. A., Gonzalez, M. I., & Long, J. R. M_2 (m-dobdc)(M= Mn, Fe, Co, Ni) metal–organic frameworks as highly selective, high-capacity adsorbents for olefin/paraffin separations. *J. Am. Chem. Soc.* 2017, 139(43), 15363-15370.

[3] Connolly, B. M., Aragones-Anglada, M., Gandara-Loe, J., Danaf, N. A., Lamb, D. C., Mehta, J. P., ... & Wheatley, A. E. Tuning porosity in macroscopic monolithic metal-organic frameworks for exceptional natural gas storage. *Nat. Commun.* 2019, 10(1), 1-11.

[4] Cadiau, A., Adil, K., Bhatt, P. M., Belmabkhout, Y., & Eddaoudi, M. A metal-organic framework–based splitter for separating propylene from propane. *Science*, 2016, 353(6295), 137-140.

[5] Horcajada, P., Chalati, T., Serre, C., Gillet, B., Sebrie, C., Baati, T., ... & Chang, J. S. Porous metal–organic-framework nanoscale carriers as a potential platform for drug delivery and imaging. *Nat. Mater.* 2010, 9(2), 172-178.

[6] Zhuang, J., Kuo, C. H., Chou, L. Y., Liu, D. Y., Weerapana, E., & Tsung, C. K. Optimized metal–organic-framework nanospheres for drug delivery: evaluation of small-molecule encapsulation. *ACS nano*, 2014, 8(3), 2812-2819.

[7] Huang, Y. B., Liang, J., Wang, X. S., & Cao, R. (2017). Multifunctional metal–organic framework catalysts: synergistic catalysis and tandem reactions. *Chem. Soc. Rev.* 2017, 46(1), 126-157.

[8] Gascon, J., Corma, A., Kapteijn, F., & Llabres i Xamena, F. X. Metal organic framework catalysis: quo vadis?. *Acs Catalysis*, 2014, 4(2), 361-378.

[9] Li, P. Z., Wang, X. J., Liu, J., Lim, J. S., Zou, R., & Zhao, Y. A triazole-containing metal–organic framework as a highly effective and substrate size-dependent catalyst for CO_2 conversion. *J. Am. Chem. Soc.* 2016, 138(7), 2142-2145.

[10] Aggarwal, H.; Bhatt, P. M.; Bezuidenhout, C. X.; Barbour, L. J. Direct evidence for single-crystal to single-crystal switching of degree of interpenetration in a metal-organic framework. *J. Am. Chem. Soc.* 2014, 136, 3776–3779.

[11] Chaemchuen, S., Zhou, K., Yusubov, M. S., Postnikov, P. S., Klomkliang, N., & Verpoort, F. Solid-state transformation in porous metal-organic frameworks based on polymorphic-pillared net structure: Generation of tubular shaped MOFs. *Micro. Meso. Mater.* 2019, 278, 99-104.

[12] Wei, R. J.; Huo, Q.; Tao, J.; Huang, R. B.; Zheng, L. S. Spincrossover FeII 4 squares: Two-step complete spin transition and reversible single-crystal-to-single-crystal transformation. *Angew. Chem., Int. Ed.* 2011, 50, 8940–8943.

[13] Yan, Z. H.; Li, X. Y.; Liu, L. W.; Yu, S. Q.; Wang, X. P.; Sun, D. Single-crystal to single-crystal phase transition and segmented thermochromic luminescence in a dynamic 3D interpenetrated AgI coordination network. *Inorg. Chem.* 2016, 55, 1096–1101.

[14] Chaemchuen, S.; Zhou, K.; Yusubov, M. S.; Postnikov, P. S.; Klomkliang, N.; Verpoort, F. Solid-state transformation in porous metal-organic frameworks based on polymorphic-pillared net structure:

Generation of tubular shaped MOFs. *Micro. Meso. Mater.* 2019, 278, 99–104.

[15] Schweighauser, L.; Harano, K.; Nakamura, E. Experimental study on interconversion between cubic MOF-5 and square MOF-2 arrays. *Inorg. Chem. Commun.* 2017, 84, 1–4.

[16] Xing, J. F.; Schweighauser, L.; Okada, S.; Harano, K.; Nakamura, E. Atomistic structures and dynamics of prenucleation clusters in MOF-2 and MOF-5 syntheses. *Nat. Commun.* 2019, 10, 3608.

[17] Guha, S.; Saha, S. Fluoride ion sensing by an anion–π interaction. *J. Am. Chem. Soc.* 2010, 132, 17674–17677.

[18] Shin, J. W.; Eom, K.; Moon D. J. *Synchrotron Rad.* 2016, 23, 369-373

[19] Otwinowski, Z.; Minor, W.; Carter Jr, C. W.; Sweet (Eds.), R. M. Methods in Enzymology 276 Part A; Academic Press: New York, 1997; 307-326.

[20] Sheldrick, G. M. SHELXT–Integrated space-group and crystal-structure determination. *Acta Crystallographica Section A: Foundations and Advances*, 2015. 71(1), 3-8.

[21] Sheldrick, G. M. SHELXT–Integrated space-group and crystal-structure determination. *Acta Crystallographica Section A: Foundations and Advances*, 2015. 71(1), 3-8.

[22] Spek, A. L. *Acta Cryst.* 2015, D65, 148-155.

[23] Hirai, K.; Reboul, J.; Morone, N.; Heuser, J. E.; Furukawa, S.; Kitagawa, S. Diffusion-coupled molecular assembly: Structuring of coordination polymers across multiple length scales. *J. Am. Chem. Soc.* 2014, 136, 14966–14973.

[24] Hosono, N.; Terashima, A.; Kusaka, S.; Matsuda, R.; Kitagawa, S. Highly responsive nature of porous coordination polymer surfaces imaged by in situ atomic force microscopy. *Nat. Chem.* 2019, 11, 109–116.

[25] Furukawa, S; Hirai, K.; Takashima, Y.; Nakagawa, K.; Kondo, M.; Tsuruoka, T.; Sakata, O.; Kitagawa, S. A block PCP crystal: Anisotropic hybridization of porous coordination polymers by face-selective epitaxial growth. *Chem. Commun.* 2009, 5097–5099.

[26] Rosi, N. L.; Eckert, J.; Eddaoudi, M.; Vodak, D. T.; Kim, J.; O'Keeffe, M.; Yaghi, O. M. Hydrogen storage in microporous metal-organic frameworks. *Science* 2003, 300, 1127–1129.

[27] Chen, B. L.; Liang, C. D.; Yang, J.; Contreras, D. S.; Clancy, Y. L.; Lobkovsky, E. B.; Yaghi, O. M.; Dai, S. A microporous metal-organic framework for gas-chromatographic separation of alkanes. *Angew. Chem., Int. Ed.* 2006, 45, 1390–1393.

[28] Chun, H.; Dybtsev, D. N.; Kim, H.; Kim, K. Synthesis, X-ray crystal structures, and gas sorption properties of pillared square grid nets based on paddle-wheel motifs: Implications for hydrogen storage in porous materials. *Chem.—Eur. J.* 2005, 11, 3521–3529.

[29] Lee, S. J.; Doussot, C.; Baux, A.; Liu, L. J.; Jameson, G. B.; Richardson, C.; Pak, J. J.; Trousselet, F.; Coudert, F. X.; Telfer, S. G. Multicomponent metal-organic frameworks as defect-tolerant materials. *Chem. Mater.* 2016, 28, 368–375.

[30] Yu, D. B.; Shao, Q.; Song, Q. J.; Cui, J. W.; Zhang, Y. L.; Wu, B.; Ge, L.; Wang, Y.; Zhang, Y.; Qin, Y. Q. et al. A solvent-assisted ligand exchange approach enables metal-organic frameworks with

diverse and complex architectures. *Nat. Commun.* 2020, 11, 927.

[31] Bai, S. Z.; Zhang, W. Q.; Ling, Y.; Yang, F. L.; Deng, M. L.; Chen, Z. X.; Weng, L. H.; Zhou, Y. M. Predicting and creating 7-connected Zn4O vertices for the construction of an exceptional metal-organic framework with nanoscale cages. *CrystEngComm.* 2015, 17, 1923– 1926.

[32] Karagiaridi, O.; Bury, W.; Tylianakis, E.; Sarjeant, A. A.; Hupp, J. T.; Farha, O. K. Opening metal-organic frameworks vol. 2: Inserting longer pillars into pillared-paddlewheel structures through solventassisted linker exchange. *Chem. Mater.* 2013, 25, 3499–3503.

[33] Swain, M. Chemicalize.org. J. *Chem. Inf. Model.* 2012, 52, 613–615.

[34] Chen, B. L.; Liang, C. D.; Yang, J.; Contreras, D. S.; Clancy, Y. L.; Lobkovsky, E. B.; Yaghi, O. M.; Dai, S. A microporous metal-organic framework for gas-chromatographic separation of alkanes. *Angew. Chem., Int. Ed.* 2006, 45, 1390–1393.

[35] Chun, H.; Dybtsev, D. N.; Kim, H.; Kim, K. Synthesis, X-ray crystal structures, and gas sorption properties of pillared square grid nets based on paddle-wheel motifs: Implications for hydrogen storage in porous materials. *Chem.—Eur. J.* 2005, 11, 3521–3529.

[36] Shekhah, O.; Wang, H.; Paradinas, M.; Ocal, C.; Schüpbach, B.; Terfort, A.; Zacher, D.; Fischer, R. A.; Wöll, C. Controlling interpenetration in metal-organic frameworks by liquid-phase epitaxy. *Nat. Mater.* 2009, 8, 481–484.

[37] Jiang, H. L.; Makal, T. A.; Zhou, H. C. Interpenetration control in metal-organic frameworks for functional applications. *Coord. Chem. Rev.* 2013, 257, 2232–2249.

[38] Ding, M. L.; Cai, X. C.; Jiang, H. L. Improving MOF stability: Approaches and applications. *Chem. Sci.* 2019, 10, 10209–10230.

[39] Pan, Y., Ding, Q., Xu, H., Shi, C., Singh, A., Kumar, A., & Liu, J. A new Zn (ii)-based 3D metal–organic framework with uncommon sev topology and its photocatalytic properties for the degradation of organic dyes. *CrystEngComm*. 2019. 21(31), 4578-4585.

[40] Bai, S. Z.; Zhang, W. Q.; Ling, Y.; Yang, F. L.; Deng, M. L.; Chen, Z. X.; Weng, L. H.; Zhou, Y. M. Predicting and creating 7-connected Zn4O vertices for the construction of an exceptional metal-organic framework with nanoscale cages. *CrystEngComm*. 2015, 17, 1923– 1926.

[41] Duan, J. G.; Higuchi, M.; Kitagawa, S. Predesign and systematic synthesis of 11 highly porous coordination polymers with unprecedented topology. *Inorg. Chem.* 2015, 54, 1645–1649.

[42] Qiu, Y. C.; Yuan, S.; Li, X. X.; Du, D. Y.; Wang, C.; Qin, J. S.; Drake, H. F.; Lan, Y. Q.; Jiang, L.; Zhou, H. C. Face-sharing archimedean solids stacking for the construction of mixed-ligand metal-organic frameworks. *J. Am. Chem. Soc.* 2019, 141, 13841–13848.

[43] He, W. W.; Li, S. L.; Yang, G. S.; Lan, Y. Q.; Su, Z. M.; Fu, Q. Controllable synthesis of a non-interpenetrating microporous metalorganic framework based on octahedral cage-like building units for highly efficient reversible adsorption of iodine. *Chem. Commun.* 2012, 48, 10001–10003.

[44] Mondloch, J. E., Bury, W., Fairen-Jimenez, D., Kwon, S., DeMarco, E. J., Weston, M. H., ... & Farha, O. K. Vapor-phase metalation by atomic layer deposition in a metal–organic framework. *Journal of the American Chemical Society*, 2013, 135(28), 10294-10297.

[45] Kung, C. W., Wang, T. C., Mondloch, J. E., Fairen-Jimenez, D., Gardner, D. M., Bury, W., ... & Wasielewski, M. R. Metal–organic framework thin films composed of free-standing acicular nanorods exhibiting reversible electrochromism. *Chemistry of Materials*, 2013, 25(24), 5012-5017.

[46] Lyu, J., Zhang, X., Otake, K. I., Wang, X., Li, P., Li, Z., ... & Bai, P. Topology and porosity control of metal–organic frameworks through linker functionalization. *Chem. Sci.* 2019, 10(4), 1186-1192.

[47] Zhang, Y. B., Furukawa, H., Ko, N., Nie, W., Park, H. J., Okajima, S., ... & Yaghi, O. M. Introduction of functionality, selection of topology, and enhancement of gas adsorption in multivariate metal–organic framework-177. *J. Am. Chem. Soc.* 2015, 137(7), 2641-2650.

[48] Dau, P. V., Tanabe, K. K., & Cohen, S. M. Functional group effects on metal–organic framework topology. *Chemical Communications*, 2012, 48(75), 9370-9372.

[49] Wang, H., Dong, X., Lin, J., Teat, S. J., Jensen, S., Cure, J., ... & Olson, D. H. Topologically guided tuning of Zr-MOF pore structures for highly selective separation of C6 alkane isomers. *Nat. Commun.* 2018, 9(1), 1-11.

[50] Pang, J., Yuan, S., Qin, J., Liu, C., Lollar, C., Wu, M., ... & Hong, M. Control the structure of Zr-tetracarboxylate frameworks through steric tuning. *J. Am. Chem. Soc.* 2017, 139(46), 16939-16945.

[51] Garibay, S. J., Iordanov, I., Islamoglu, T., DeCoste, J. B., & Farha, O. K. Synthesis and functionalization of phase-pure NU-901 for enhanced CO_2 adsorption: the influence of a zirconium salt and modulator on the topology and phase purity. *CrystEngComm*, 2018, 20(44), 7066-7070.

[52] Ma, J., Tran, L. D., & Matzger, A. J. Toward topology prediction in zr-based microporous coordination polymers: the role of linker geometry and flexibility. *Crystal Growth & Design*, 2016, 16(7), 4148-4153.

[53] Hawxwell, S. M., Adams, H., & Brammer, L. Two-dimensional metal-organic frameworks containing linear dicarboxylates. *Acta Crystallographica Section B: Structural Science*, 2006. 62(5), 808-814.

[54] Wu, Y., Breeze, M. I., O'Hare, D., & Walton, R. I. High energy X-rays for following metal-organic framework formation: Identifying intermediates in interpenetrated MOF-5 crystallisation. *Microporous and Mesoporous Materials*, 2017. 254, 178-183.

[55] Peng, Q., Qiao, Y., Kannari, K., Ge, A., Inoue, K. I., & Ye, S. In situ spectroscopic investigations of electrochemical oxygen reduction and evolution reactions in cyclic carbonate electrolyte solutions. *The Journal of Physical Chemistry C*, 2020, 124(29), 15781-15792.

[56] Chai, J., Liu, Z., Zhang, J., Sun, J., Tian, Z., Ji, Y., ... & Cui, G. A superior polymer electrolyte with rigid cyclic carbonate backbone for rechargeable lithium ion batteries. *ACS applied materials & interfaces*, 2017, 9(21), 17897-17905.

[57] Bai, D., Wang, Q., Song, Y., Li, B., & Jing, H. Synthesis of cyclic carbonate from epoxide and CO_2 catalyzed by magnetic nanoparticle-supported porphyrin. *Catalysis Communications*, 2011, 12(7), 684-688.

[58] Yuan, Y., Li, J., Sun, X., Li, G., Liu, Y., Verma, G., & Ma, S. Indium–Organic Frameworks Based on Dual Secondary Building Units Featuring Halogen-Decorated Channels for Highly Effective

CO_2 .Fixation. *Chemistry of Materials*, 2019. 31(3), 1084-1091.

[59] Li, P. Z., Wang, X. J., Liu, J., Lim, J. S., Zou, R., & Zhao, Y. A triazole-containing metal–organic framework as a highly effective and substrate size-dependent catalyst for CO_2 conversion. *Journal of the American Chemical Society*, 2016, 138(7), 2142-2145.

[60] Kathalikkattil, A. C., Babu, R., Roshan, R. K., Lee, H., Kim, H., Tharun, J., ... & Park, D. W. An lcy-topology amino acid MOF as eco-friendly catalyst for cyclic carbonate synthesis from CO_2: Structure-DFT corroborated study. *Journal of Materials Chemistry A*, 2015, 3(45), 22636-22647.

[61] Babu, R., Kathalikkattil, A. C., Roshan, R., Tharun, J., Kim, D. W., & Park, D. W. Dual-porous metal organic framework for room temperature CO_2 fixation via cyclic carbonate synthesis. *Green Chemistry*, 2016, 18(1), 232-242.

[62] Zou, R., Li, P. Z., Zeng, Y. F., Liu, J., Zhao, R., Duan, H., ... & Zhao, Y. Bimetallic Metal-Organic Frameworks: Probing the Lewis Acid Site for CO_2 Conversion. *Small*, 2016, 12(17), 2334-2343.

[63] Gao, W. Y., Tsai, C. Y., Wojtas, L., Thiounn, T., Lin, C. C., & Ma, S. Interpenetrating metal–metalloporphyrin framework for selective CO2 uptake and chemical transformation of CO_2. *Inorganic chemistry*, 2016, 55(15), 7291-7294.

[64] CherianáKathalikkattil, A., & JuneáCho, S. A sustainable protocol for the facile synthesis of zinc-glutamate MOF: an efficient catalyst for room temperature CO_2 fixation reactions under wet conditions. *Chemical Communications*, 2016, 52(2), 280-283.

[65] Gao, W. Y., Tsai, C. Y., Wojtas, L., Thiounn, T., Lin, C. C., & Ma, S. Interpenetrating metal–metalloporphyrin framework for selective CO2 uptake and chemical transformation of CO_2. *Inorganic chemistry*, 2016, 55(15), 7291-7294.

[66] Kong, L. D.; Zou, R. Y.; Bi, W. Z.; Zhong, R. Q.; Mu, W. J.; Liu, J.; Han, R. P. S.; Zou, R. Q. Selective adsorption of CO2/CH4 and CO2/N2 within a charged metal-organic framework. *J. Mater. Chem. A* 2014, 2, 17771–17778.

[67] Shang, J.; Li, G.; Singh, R.; Gu, Q. F.; Nairn, K. M.; Bastow, T. J.; Medhekar, N.; Doherty, C. M.; Hill, A. J.; Liu, J. Z. et al. Discriminative separation of gases by a "molecular trapdoor" mechanism in chabazite zeolites. *J. Am. Chem. Soc.* 2012, 134, 19246–19253.

[68] Jiang, T., Zhou, Y., Liang, S., Liu, H., & Han, B. Hydrogenolysis of glycerol catalyzed by Ru-Cu bimetallic catalysts supported on clay with the aid of ionic liquids. *Green Chemistry*, 2009. 11(7), 1000-1006.

[69] Noh, J., Kim, D., Lee, J., Yoon, M., Park, M. H., Lee, K. M., ... & Kim, M. Three Component Controls in Pillared Metal-Organic Frameworks for Catalytic Carbon Dioxide Fixation. *Catalysts*, 2018, 8(11), 565.

[70] Zhu, M., Wu, J., Wang, Y., Song, M., Long, L., Siyal, S. H., ... & Sui, G. Recent advances in gel polymer electrolyte for high-performance lithium batteries. Journal of Energy Chemistry, 2009, 37, 126-142.

Acknowledgement

I would like to give thanks to all who helped me to conduct my master's program at the Ulsan Nation Institute of Science and Technology.

I appreciate professor Hoi Ri Moon. During my master's program, she taught me how to progress my research and the attitude I should have as a chemist. Thanks to her careful supervision, I was able to resolve some problems I faced during my research and make meaningful research results. I appreciate professor Myoung Soo Lah, Wonyoung Choe who were the committee members of my dissertation. Thanks to them, I could review my research capability I raised during my master's program and think about how to develop my research topic.

I appreciate my lab members – Jae Hwa Lee, Junsu Ha, Sujee Cho, HongKyu Lee, and Doo Hwan Hong. Whenever I asked them for some advice about my research, they actively gave their help to me and inspiration to develop my research. Thanks to them, I was able to develop my capability of progressing my research.

I appreciate my dear family who sincerely gives their love for me. My mother Jeong Ja Bae always shows her enthusiasm for her own study instead of lecturing me. Her such enthusiasm inspired me to have enthusiasm for studying whatever I want. My older brother Jaewan Kim always root for me without forcing what he wants. Thanks to him, I was able to pave my way in which I want to go.

My friend MyeongJung Kim give loves me without any prejudice. He is always with me whenever I was in trouble and helps me to overcome the trouble. I will also be with him whenever he was in trouble for him to make him keep his current pureness! My friend Hongyoung Choe is always sincerely treating me and encourages me to keep myself. Thanks to her cheerful mindset, I was able to become happy. I will be her sincere friend whether she was in a happy or hard situation. Besides the above people, I have plenty of people - my dear friends, and teachers - to whom I have thankfulness. Even though I cannot express my thankfulness to each person, I sincerely love all of them and thanks.